

# Linear nonadiabatic properties of SX Phoenicis variables

P. Santolamazza<sup>1</sup>, M. Marconi<sup>1</sup>, G. Bono<sup>2</sup>, F. Caputo<sup>2</sup>, S. Cassisi<sup>3</sup> and R. L. Gilliland<sup>4</sup>

## ABSTRACT

We present a detailed linear, nonadiabatic pulsational scenario for oscillating Blue Stragglers (BSs)/SX Phoenicis (SX Phe) in Galactic Globular Clusters (GGCs) and in Local Group (LG) dwarf galaxies. The sequences of models were constructed by adopting a wide range of input parameters and properly cover the region of the HR diagram in which these objects are expected to be pulsationally unstable. Current calculations together with more metal-rich models already presented by Gilliland et al. suggest that the pulsation properties of SX Phe are partially affected by metal content. In fact, the pulsation periods for the first three modes are marginally affected when moving from  $Z=0.0001$  to  $0.006$ , whereas the hot edges of the instability region move toward cooler effective temperatures by approximately  $300 \div 500$  K.

The inclusion of a metallicity term in the Period-Luminosity-Color (PLC) relations causes a substantial decrease in the intrinsic scatter and in the individual error of the coefficients. This supports the result recently brought out by Petersen & Christensen-Dalsgaard for  $\delta$  Scuti stars. Moreover, we find that the discrepancy between our relation and similar theoretical and empirical relations available in the literature is typically smaller than 5%. The comparison between theory and observations in the  $M_V - \log P$  plane as well as in the luminosity amplitude  $-\log P$  plane does not help to disentangle the long-standing problem of mode identification among SX Phe stars. However, our calculations suggest that the secular period change seems to be a good observable to identify the pulsation mode of cooler SX Phe variables.

Together with the previous models we also constructed new sequences of models by adopting selected effective temperatures and luminosities along two

---

<sup>1</sup>Osservatorio Astronomico di Capodimonte, Via Moiariello 16, 80131 Napoli, Italy; patrizia@na.astro.it; marcella@na.astro.it

<sup>2</sup>Osservatorio Astronomico di Roma, Via Frascati 33, 00040 Monte Porzio Catone, Italy; bono@coma.mporzio.astro.it, caputo@coma.mporzio.astro.it

<sup>3</sup>Osservatorio Astronomico di Collurania, Via M. Maggini, 64100 Teramo, Italy; cassisi@astrte.te.astro.it

<sup>4</sup>Space Telescope Science Institute, 3700 San Martin Drive, Baltimore, MD 21218; gillil@stsci.edu

evolutionary tracks characterized by the same mass value and metal content ( $M/M_{\odot}=1.2$ ,  $Z=0.001$ ) but different He contents in the envelope, namely  $Y=0.23$  and  $Y=0.30$ . The He content in the latter track was artificially enhanced soon after the central H exhaustion to mimic, with a crude approximation, the collisional merging between two stars. Interestingly enough, we find that the He-enhanced models present an increase in the pulsation period and a decrease in the total kinetic energy of the order of 20% when compared with the canonical ones. At the same time, the blue edge of the fundamental mode for the He-enhanced models is approximately 1,000 K cooler than for canonical ones. Moreover, we find that the secular period change for He-enhanced models is approximately a factor of two larger than for canonical ones. According to this evidence we suggest that the pulsation properties of SX Phe can be soundly adopted to constrain the evolutionary history of BSs, and in turn to single out the physical mechanisms which trigger their formation.

*Subject headings:*  $\delta$  Scuti – stars: blue stragglers – stars: evolution – stars: oscillations  
– stars: variables: other

## 1. Introduction

During the last few years both ground based and HST photometric observations of Open Clusters (Ahumada, & Lapasset 1995; Dinescu et al. 1996; Landsman et al. 1998; Mazur et al. 1999b), GGCs (Auriere, Lauzeral, & Ortolani 1990; Buonanno et al. 1994; Ferraro, Fusi Pecci, & Bellazzini 1995; Walker & Nemeč 1996; Kaluzny et al. 1997; Guarnieri et al. 1998; Borissova et al. 1999; Ferraro et al. 1999; Piotto et al. 1999), and dwarf Spheroidal galaxies (dSphs, Mateo et al. 1995; Grillmair et al. 1998; Monikiewicz et al. 1999) brought out the evidence that BSs are more a widespread feature than an anomaly in these stellar systems. The BSs are systematically bluer than cluster main-sequence (MS) stars and typically cover a range of two magnitudes above the Turn-Off (TO). Therefore BSs in these stellar systems mimic a population of MS and post-MS stars more massive than the TO stars. The observational scenario of these intriguing objects is further enriched by the fact that BSs cross the Cepheid instability strip, and therefore a fraction of them, roughly the 30%, oscillate both in radial and/or nonradial modes (Gilliland et al. 1998, hereinafter G98). The oscillating BSs after the discovery in  $\omega$  Cen (Niss 1981) were christened SX Phoenicis variables (Nemeč & Mateo 1990).

The BSs are the crossroad of paramount theoretical and observational efforts, since we still lack a firm understanding of the physical processes that govern their origin and their subsequent evolution. Even though several mechanisms have been proposed to explain the occurrence of BSs in GCs, we have not yet understood how the dynamical history of the cluster cores affects the formation of these objects. The most popular mechanism suggested for the formation of BSs is the mass accretion of a MS star caused either by the mass transfer/coalescence between different components in primordial binary systems (binary merging) or the direct collision of two or more stars (collisional merging) in high density regions (Bailyn 1995; Sandquist, Bolte, & Hernquist 1997, hereinafter SBH97; Sills & Bailyn 1999). These two different hypotheses have been further strengthened by the discovery of contact, semidetached, and detached eclipsing binaries in several GCs (Mateo et al. 1990; Kaluzny, & Krzeminski 1993; Edmonds et al. 1996; Rubenstein, & Bailyn 1996; Yan & Reid 1996; Mazur, Kaluzny, & Krzeminski 1999a, and references therein).

Moreover, dynamical calculations suggest that the binding energy in primordial binaries is a key source to prevent, if not halt, the core collapse and/or to trigger the expansion during the post-core collapse phases. As a consequence, if BSs are formed via a binary merging, the luminosity function of BSs can constrain the energy supplied by these objects (SBH97). On the other hand, if BSs are the progeny of star-star, binary-star, or binary-binary interactions, then the luminosity functions of clusters characterized by different central densities can supply tight constraints on the cross section of stellar

interactions (SBH97).

In order to properly identify binary and collisional BSs, Baily (1992) suggested a photometric criterion. In fact, hydrodynamical calculations by Benz & Hills (1992) show that the remnants of two colliding stars are characterized by a higher He content in the envelope than the remnants of binary merging. As a consequence, the BSs formed via collisional merging should be simultaneously brighter and bluer than the ones formed via binary merging. The difference in the chemical profile would also imply a substantial change in the evolutionary tracks and in the luminosity functions of the two BSs groups (Baily & Pinsonneault 1995; SBH97). A further interesting observable to split binary and collisional BSs has been suggested by Shara, Saffer, & Livio (1997) and by Ouellette, & Pritchett (1998) who noted that the remnants of collisional mergings should be, due to the conservation of angular momentum, rapidly rotating stars.

Although these selection criteria appear to be based on straightforward empirical stellar properties and an unprecedented number of BSs stars have been detected by HST observations in the dense cores of GGCs we still lack a clear understanding on the intimate nature of these objects. In fact, recent deep photometric data support the evidence that BSs present a bimodal radial distribution (Baily, & Pinsonneault 1995; Ferraro et al. 1997; Saviane et al. 1998). In this scenario the BSs located close to cluster center were formed via stellar collisions, whereas the BSs located in the outskirts of the cluster formed via binary merging. However, no general consensus has been reached yet, and indeed Sigurdsson et al. (1994) suggested that the entire sample of BSs in M3 formed via stellar collisions, while Sills, & Baily (1999) suggested that in this cluster the BSs centrally located are the progeny of two distinct populations.

In view of these unquestionable facts, we suggest to investigate the pulsation behavior of SX Phe variables to constrain the physical mechanisms that trigger the formation and evolution of BSs. In fact, it has been recently shown (Petersen & Christensen-Dalsgaard 1996; G98; Petersen & Hög 1998a) that the comparison between predicted and observed period ratios can supply useful constraints on the pulsation masses of mixed-mode variables. Interestingly enough, G98 found a good agreement between pulsational and evolutionary masses for 4 mixed-mode variables and by combining the two estimates it turned out that the stellar masses of these objects range from  $1.3 \pm 0.1$  to  $1.6 \pm 0.2 M_{\odot}$ . Although this approach presents several advantages, the theoretical predictions currently adopted in the literature to constrain the pulsational behavior of SX Phe are only based on linear adiabatic and nonadiabatic models. Therefore the comparison between theory and observations was limited to period and period ratios. At the same time, the mode identification was based on linear growth rates instead of on nonlinear limit cycles. This is the second paper of a

series devoted to a detailed theoretical and observational analysis of SX Phe variables in stellar systems and in the Galactic field.

The main aim of this investigation is to present new linear, nonadiabatic pulsation models for metal-poor ( $Z=0.0001$  and  $Z=0.001$ ) SX Phe and to compare theoretical predictions with observational data available in the literature. In §2 we discuss current linear, nonadiabatic models and present a detailed analysis of the dependence of pulsation properties on metallicity. In §3.1 we supply the analytical relations for the first three radial modes connecting the pulsation period to stellar mass, luminosity, effective temperature, and metallicity. Both the PLC and the PLCZ relations and their intrinsic accuracies are detailed in §3.2, together with the comparison with similar theoretical and empirical relations available in the literature. The comparison between the predicted blue edges for the first three radial modes with current empirical data on SX Phe in GGCs, in dwarf galaxies, and in the Galactic field is presented in §4. In this section the problems that are still hampering the mode identification among SX variables are also briefly discussed. The dependence of modal stability, and pulsation periods on the He content is presented in §5. The impact that the comparison between empirical and theoretical observables could provide to disentangle the evolutionary history of BSs are also outlined in this section. The main results of this investigation are summarized in §6.

## 2. Linear Nonadiabatic Models

The input physics, physical and numerical assumptions adopted to construct linear, nonadiabatic, radiative models for SX Phe variables were already addressed in Bono et al. (1997, hereinafter B97) and in G98. Therefore they are not discussed in detail here. In order to supply a comprehensive theoretical framework for SX Phe in GGCs we constructed several sequences of models by adopting a fixed He content ( $Y=0.24$ ) and two different metal abundances, namely  $Z=0.0001$  and  $Z=0.001$ . For each given chemical composition we adopted three different mass values ( $M/M_{\odot}=1.0, 1.2, 1.4$ ) and luminosity levels ranging from  $\log L/L_{\odot} = 0.60$  to  $\log L/L_{\odot} = 1.4$ . The models cover a wide temperature range ( $6,000 \leq T_e \leq 8,800$  K) and for each individual model we investigated the modal stability of the first three radial modes.

Tables 1-3<sup>5</sup> summarize the input parameters and selected linear observables for the entire set of models we constructed. From left to right the columns give: luminosity, effective temperature (K), radius (cm), period (day), pulsation constant (d), kinetic energy

---

<sup>5</sup>Table 1 is published in the printed edition, while Tables 2 and 3 are only available in the on-line edition.

(ergs), and growth rate. The third column of Tables 2 and 3 lists the first overtone (FO) and the second overtone (SO) to fundamental (F) period ratios respectively. In agreement with the assumption adopted by G98 the inner boundary was fixed at a relative distance from the stellar center roughly equal to 10 % of the photospheric radius. This choice ensures that the envelope mass throughout the instability strip ranges from 40 to 80% of the total mass. The mass ratios between consecutive zones and the spatial resolution across the envelope were also fixed according to G98. For temperatures higher than 10,000 K we adopted OPAL radiative opacities (Iglesias & Rogers 1996), while for lower temperatures we adopted molecular opacities by Alexander & Ferguson (1994). The procedure adopted to interpolate the opacity tables is described in Bono, Incerpi, & Marconi (1996). The small values attained by the growth rate explains why up to now the lengthy calculations necessary to investigate the nonlinear behavior of high gravity variables have been only partially tackled (Bono et al. 1997).

Figure 1 shows the opacity and the adiabatic exponent  $\Gamma_3$  (left panels) as a function of logarithmic temperature for three different models centrally located in the instability strip. These models were constructed by adopting the same stellar mass ( $M/M_\odot=1.2$ ), luminosity ( $\log L/L_\odot=1.05$ ), effective temperature ( $T_e = 7250$  K), and He content ( $Y=0.24$ ) but three different metal abundances, namely 0.0001, 0.001, and 0.006. Data plotted in this figure show quite clearly that these structures present a mild dependence on metal content, and indeed a decrease of almost 1.5 dex in  $[\text{Fe}/\text{H}]$  causes a decrease of the order of 20% in the Z-bump opacity ( $\log T \approx 5.15$ ) and a negligible change in both HeII ( $\log T \approx 4.65$ ) and H plus HeI ( $\log T \approx 4.18$ ) opacity peaks. The adiabatic exponent also shows a negligible dependence on  $Z$ , and indeed the three models attain, in this temperature interval, almost identical values. The mild dependence on  $Z$  is also supported by F periods which increase by approximately 3% when moving from  $Z=0.0001$  to 0.006.

The total works plotted in the right panels show, as expected (Bono, Marconi & Stellingwerf 1999a), that an increase in the metal content from 0.0001 to 0.006 causes a decrease in the pulsation destabilization. In fact, the total work of the F mode decreases from  $7.15 \times 10^{-6}$  ( $Z=0.0001$ ) to  $3.80 \times 10^{-6}$  ( $Z=0.006$ ). Even though the Z-bump in the more metal-rich model (dashed line) is larger than in the metal-poor ones (solid line) the driving across this region is smaller in the former model than in the latter ones. This effect might be due to the fact that the opacity derivatives in the more metal-rich model are smoother than in the metal-poor ones. The FO mode shows a similar behavior, and indeed the pulsation periods increase by less than 1%, while the total work decreases from  $7.97 \times 10^{-5}$  ( $Z=0.0001$ ) to  $5.02 \times 10^{-5}$  ( $Z=0.006$ ). We refer the reader to G98 for a detailed discussion on the role played by the Z-bump and by the location of radius, luminosity and temperature nodes in the destabilization of overtone pulsators. Note that even though the

dependence of the SX Phe pulsation properties on metallicity is marginal, an increase in the metal content causes a shift of the fundamental blue edge (FBE) toward cooler effective temperatures by approximately 200 K at  $\log L/L_{\odot}=1.0$  and 500 K at  $\log L/L_{\odot}=0.7$ . In this luminosity range first and second overtone blue edges move toward lower effective temperatures by roughly 400 K. This suggests that metal-poor BSs are, at fixed input parameters, more enthusiastic pulsators than metal-rich ones.

The small values attained by the quoted total works together with the values listed in column (7) of Tables 1-3 confirm the strong adiabatic nature of SX Phe brought out by G98. Current results also suggest that at fixed input parameters a decrease in metallicity causes a further decrease in the total work, and in turn in the adiabatic nature of these objects. The normalized total work is the analog of the growth rate, i.e. the stability parameter which supplies a necessary condition for the modal stability. A glance at the models which are unstable in the first three modes suggests that the SO total works are higher than for FO and the latter ones higher than for F pulsators. This finding confirms that even in the metal-poor regime higher overtones are more destabilized than the F mode (G98). Moreover, the evidence that at fixed input parameters the total kinetic energy decreases by approximately a factor of 5 between F and FO and by a factor of 2.5 between first and second overtone makes the probability to detect overtone pulsators among SX Phe higher than for F ones. Finally, we mention that a decrease in the metal content causes on average an increase in the period ratio. In fact, the  $P_1/P_0$  increases from 0.77 to 0.79 when moving from  $Z=0.006$  to  $Z=0.0001$ . The difference among higher overtones is smaller, and indeed the same change in metallicity causes an increase in  $P_2/P_1$  from 0.81 to 0.82. The small changes in the period ratios of consecutive models listed in Table 2-3 are caused by marginal variations in the total mass of the envelope.

### 3. Systematic pulsation properties

#### 3.1. Pulsation periods

Recent optical and UV data collected with HST allowed the identification and the follow-up of exotic X-ray sources in the core of GCs (Grindlay 1999). Quite often these objects present luminosity variations on time scales which range from few minutes to 17 hours. As a consequence, they partially cover the period range of SX Phe (Deutsch, Margon, & Anderson 2000). In order to supply the pulsation relations -i.e. the analytical relations which connect the pulsation period to stellar mass, luminosity, and effective temperature- for the first three radial modes, we estimated the least square fit to the large grid of models listed in Tables 1-3. However, the comparison between the periods based

on the new relations and the periods based on the analytical relations derived by G98 for  $Z=0.006$  presents a period difference that for the second overtone is the of order of 0.015 in  $\log P$ . Therefore, to derive pulsation relations which cover a wide metallicity range ( $0.0001 \leq Z \leq 0.006$ ) we performed once again the fit by including the G98 models. The analytical relations we find are the following:

$$\begin{aligned} \log P(F) &= 9.854(\pm 0.003) - 0.434(\pm 0.005) \cdot \log M + 0.743(\pm 0.001) \cdot \log L \\ &\quad - 3.016(\pm 0.005) \cdot \log T_e + 0.0023(\pm 0.0004) \cdot \log Z \quad \sigma = 0.003 \\ \log P(FO) &= 9.800(\pm 0.004) - 0.401(\pm 0.006) \cdot \log M + 0.736(\pm 0.001) \cdot \log L \\ &\quad - 3.034(\pm 0.006) \cdot \log T_e + 0.0043(\pm 0.0005) \cdot \log Z \quad \sigma = 0.004 \\ \log P(SO) &= 9.620(\pm 0.004) - 0.382(\pm 0.006) \cdot \log M + 0.725(\pm 0.001) \cdot \log L \\ &\quad - 3.011(\pm 0.005) \cdot \log T_e + 0.0081(\pm 0.0004) \cdot \log Z \quad \sigma = 0.004 \end{aligned}$$

where  $M$  and  $L$  are in solar units,  $\sigma$  is the standard deviation and the other symbols have their usual meaning. Note that the sign of the metallicity term supplies a direct explanation of the empirical evidence recently brought out by Rodriguez & Lopez-Gonzalez (2000, hereinafter RLG00) that the mean period of SX Phe in GGCs and in LG dwarfs scales with the metallicity. The accuracy of the new analytical relations is further strengthened by data plotted in Figure 2 that shows the difference between computed and analytical periods for the three selected metallicities. In fact, the discrepancy for the first three modes is, over the entire period range, typically smaller than 0.005 dex.

Finally, we mention that current models have been constructed by assuming that radiation is the main flux carrier throughout the envelope. This is a plausible assumption for hot models but could introduce systematic uncertainties in the coolest ones. In order to supply a quantitative estimate of this effect we evaluated the difference between the periods for  $\delta$  Scuti stars predicted by B97 on the basis of both linear, nonadiabatic, radiative models and full amplitude, nonlinear, convective models (see their Tables 1 and 2). We find that the difference for the first three radial modes ranges from approximately  $9 \times 10^{-4}$  to  $2 \times 10^{-3}$ . As expected the nonlinear, convective periods are systematically shorter than the linear, radiative ones (Bono & Stellingwerf 1994). This difference might introduce spurious effects in the period ratios predicted by radiative models but it has negligible effects on individual periods. On the other hand, the assumption of radiative transport marginally affects the linear predictions on the blue edges. In fact, they are typically located at effective temperatures hotter than 7,500 K, and therefore radiation is the main flux carrier throughout the envelope. The comparison between linear and nonlinear blue edges predicted by B97 is hampered by the occurrence of mixed-mode pulsators across the



edges.

### 3.2. Theoretical Period-Luminosity-Color relations

In two recent detailed investigations McNamara (1997,2000) found that High-Amplitude  $\delta$  Scuti (HADS, i.e. variables with visual amplitudes larger than  $0.15 \div 0.30$  mag) and SX Phe stars obey to a Period-Luminosity (PL) relation. This finding was supported by Petersen & Christensen-Dalsgaard (1999, hereinafter PCD99) who also found that the intrinsic dispersion of the theoretical PL relation can be significantly reduced by including both a color and/or a metallicity term, i.e. by adopting a PLC or a PLCZ relation. It is worth mentioning that the previous authors, according to empirical evidence on the width of the instability strip, found that this outcome holds not only for HADS but also for the broad family of  $\delta$  Scuti stars.

To assess whether SX Phe pulsators follow the same trend we estimated the least square solutions for the sample of models listed in Table 1-3 and for G98 models. The analytical PLC and PLCZ relations for the first three radial modes we find are the following:

$$\begin{aligned}
 M_{bol}(F) &= 41.06 & -3.69 \log P & -11.17 \log T_e & (\sigma=0.08) \\
 &\pm 0.08 & \pm 0.03 & \pm 0.18 & \\
 M_{bol}(FO) &= 39.79 & -3.68 \log P & -10.93 \log T_e & (\sigma=0.09) \\
 &\pm 0.09 & \pm 0.03 & \pm 0.17 & \\
 M_{bol}(SO) &= 38.20 & -3.67 \log P & -10.61 \log T_e & (\sigma=0.09) \\
 &\pm 0.09 & \pm 0.02 & \pm 0.19 & 
 \end{aligned}$$

where the pulsation periods are in days, the effective temperatures in K, and the bolometric magnitudes were derived by assuming  $M_{bol}(\odot) = 4.62$  mag. The  $\sigma$  values given at the end of each relation is the intrinsic dispersion. The PLCZ relations are the following:

$$\begin{aligned}
 M_{bol}(F) &= 41.60 & -3.73 \log P & -11.37 \log T_e & -0.07 \log Z & (\sigma=0.06) \\
 &\pm 0.06 & \pm 0.02 & \pm 0.14 & \pm 0.01 & \\
 M_{bol}(FO) &= 40.87 & -3.73 \log P & -11.30 \log T_e & -0.09 \log Z & (\sigma=0.06) \\
 &\pm 0.06 & \pm 0.02 & \pm 0.12 & \pm 0.01 & \\
 M_{bol}(SO) &= 40.22 & -3.76 \log P & -11.24 \log T_e & -0.10 \log Z & (\sigma=0.06) \\
 &\pm 0.06 & \pm 0.02 & \pm 0.12 & \pm 0.01 & 
 \end{aligned}$$

Previous results support the finding brought out by PCD99, and indeed not only the errors on the coefficients but also the formal scatter of the PLCZ relations are systematically smaller than for the PLC relations. In particular, we find that the  $\sigma$  values in the former relations decrease by a factor ranging from 30% (F) to 50% (FO, SO). Note that current

relations were derived by including all unstable models i.e. no temperature selection was performed.

Figure 3 shows the fractional difference in the bolometric magnitude for the fundamental mode between our PLCZ relation and the PLCZ relations derived by PCD99 on the basis of theoretical models (triangles) and empirical data (circles) collected by McNamara (1997). The comparison was performed at fixed metallicity  $Z=0.006$ , since the metal content of the models constructed by PCD99 range from  $Z=0.005$  to  $Z=0.02$ , while the metal abundances of HADS collected by McNamara range from  $Z=0.0001$  to  $Z=0.02$ . The agreement between the three relations is remarkable, since the discrepancy is typically smaller than 5% over the entire period range. This finding leads further support to the evidence that both SX Phe and  $\delta$  Scuti can be safely adopted to estimate stellar distances. Moreover, previous PLCZ relations suggest that SX Phe pulsating in the first or in the second overtone could be good standard candles as well. In fact, the  $\sigma$  values of their PLCZ relations are, within the errors, identical to the fundamental one.

The agreement in the sign of the metallicity term in both theoretical and empirical relations brings out a key result: *metal-poor SX Phe and  $\delta$  Scuti stars are at fixed period and effective temperature fainter than metal-rich ones.* This finding is interesting not only because observations and theoretical predictions span a three dex metallicity range but also because it supports recent empirical and theoretical predictions based on the PLC (Bono et al. 1999a,b; Groenewegen 2000) and on PLCZ (Bono & Marconi 1999) of classical Cepheids<sup>6</sup>. In fact, as suggested by Fernie (1992), and more recently supported by McNamara (1997),  $\delta$  Scuti and classical Cepheids seem to follow the same PLC relations.

#### 4. Comparison between theory and observations

Up to now 122 SX Phe have been detected in 18 GGCs and 27 in two LG dwarf galaxies (Carina, Sagittarius). The metallicity of these objects ranges from  $[\text{Fe}/\text{H}]=-0.70$  (47 Tuc) to  $-2.4$  (NGC 5053). The reader interested in an overview of SX Phe observational properties is referred to the recent paper by RLG00. In order to derive a large data sample of both cluster and field SX Phe we selected among the field objects available in the literature the stars with  $[\text{Fe}/\text{H}] \leq -0.50$ , since the metallicity of our models ranges from  $Z=0.0001$  to  $Z=0.006$ . We end up with 12 field SX Phe stars.

---

<sup>6</sup> Note that in the PL plane the dependence on metallicity is exactly the contrary i.e. at fixed period metal-poor Cepheids are brighter than metal-rich ones.

The pulsation period, the absolute magnitude and the visual amplitude for the entire sample are listed in Table 4 (available in the on line edition). Note that our sample of SX Phe in GGCs is not identical to the RLG00 one. We did not include the variables G172 and H2 detected in M 4 and M 71, since they present quite different color than the bulk of SX Phe stars. We also excluded 4 SX Phe in NGC 6397, since their period is uncertain, but we included the SX Phe recently discovered by Mochejska, Kaluzny, & Thompson (2000) in E 3. At the same time, we also excluded 4 SX Phe in Carina, since only B magnitudes are available for these objects. We end up with a sample of 117 SX Phe in GGCs and with a sample of 23 SX Phe in dwarf galaxies.

The periods in the sample of SX Phe we collected range from 45 minutes to roughly 4 hours ( $\log P = -1.54 \div -0.8$ ) and V amplitudes  $A_V$  from 0.02 to 0.90 mag. In order to shed more lights on the long-standing problem of mode identification we plotted the entire sample of SX Phe in the Bailey diagram, i.e.  $A_V$  vs period. We find that these observables are useless to disentangle this problem, since over the entire period range the visual amplitudes changes from few hundredths up to tenths of magnitudes. The same outcome applies if we split the sample by adopting different metallicity bins. This suggests that in the Bailey diagram no clear separation emerge between SX Phe pulsating in the fundamental or in higher overtones.

Even though it has been generally assumed that large luminosity amplitudes ( $A_V \geq 0.15 \div 0.3$ ) are a key feature of fundamental pulsators (McNamara 1995,1997) both empirical and theoretical evidence suggest that this criterion could be affected by selection biases. In fact, current nonlinear, convective models of  $\delta$  Scuti stars (Bono et al. 1997) support the evidence that overtone pulsators present large luminosity amplitudes close to the hot edge of the instability strip, while fundamental pulsators present small amplitudes close to the cool edge. The double-mode SX Phe V2 detected in 47 Tuc (G98) presents a V amplitude equal to 0.051 in the fundamental mode. This means that a selection criterion only based on the pulsation amplitude could misidentify low-amplitude fundamental pulsators. Moreover, as already noted by G98, the detection of low-amplitude, long-period SX Phe could be affected by selection effects.

We also note that SX Phe in Carina are characterized on average by larger luminosity amplitudes  $A_V \approx 0.55$  mag when compared with the amplitudes of SX Phe in GGCs. However, this sample could be affected by potential selection effects, since the photometric accuracy at the typical mean magnitude of SX Phe in Carina was of the order of 0.05 mag (Mateo et al. 1998). On the other hand, the three SX Phe detected in Sagittarius present normal amplitudes, but unfortunately their membership has not been confirmed yet. As a consequence, current data do not allow us to assess on a firm basis what is typical from

what is peculiar, and in particular whether SX Phe in dwarf galaxies and in GGCs share the same properties.

To assess whether linear, nonadiabatic models can help to disentangle this thorny problem the theoretical blue (hot) edges of the instability strip for the first three radial modes were transformed into the observational plane by adopting the bolometric corrections provided by Castelli, Gratton & Kurucz (1997a,b). Owing to the mild dependence of the blue edges on the metal content, we derived by adopting the entire set of models -i.e. current plus G98- the following analytical relations:

$$\begin{aligned}
 M_V^B(F) &= -1.32 & -3.05 \log P & (\sigma=0.07) \\
 &\pm 0.06 & \pm 0.05 & \\
 M_V^B(FO) &= -1.88 & -3.13 \log P & (\sigma=0.05) \\
 &\pm 0.05 & \pm 0.04 & \\
 M_V^B(SO) &= -2.43 & -3.26 \log P & (\sigma=0.05) \\
 &\pm 0.06 & \pm 0.04 &
 \end{aligned}$$

where the symbols have their usual meaning. Figure 4 shows the comparison in the Magnitude-Period diagram between current empirical data in GGCs (top) and in dwarf galaxies (bottom) with the blue edges for the first three radial modes. Distance moduli and metallicities for GGCs were taken from Harris (1996) and Carretta & Gratton (1997), while for Carina and Sagittarius we adopted the values suggested by Mateo (1998). A glance at the data plotted in this figure clearly shows that the bulk of SX Phe (roughly 70%) are distributed in the so-called "OR-region" i.e. the region of the instability strip in which two or more modes are simultaneously excited. Therefore this theoretical scenario does not allow us to firmly identify the mode of these variables. However we note that, within current uncertainties on GGC distances, the variables located above the FBE are almost certainly overtone pulsators. The location of blue edges is only marginally affected by nonlinear effects and therefore the nonlinear blue edges should only be slightly shifted toward cooler effective temperatures. Moreover, the four brightest variables among the SX Phe identified in 47 Tuc are also located above the FBE, in particular the double-mode variable V15 is almost certainly pulsating in overtones higher than the second one. This evidence supports the mode identification suggested by G98 for this object. The same outcome applies for V2.

Figure 5 shows the distribution of field SX Phe in the  $M_V - \log P$  diagram. The comparison with the theoretical edges brings out the same behavior we already found for SX Phe in GGCs and in dwarfs. Three fundamental/first overtone double-mode variables have been identified to date among field SX Phe, namely BL Cam (Hintz et al. 1997a), SX Phe (Nemec, Nemec-Linnell, & Lutz 1994), and AE UMa (Hintz et al. 1997b). Note that

among these variables the main pulsation mode, i.e. the mode with the largest luminosity amplitude, is the fundamental one. Our results seem to support these identifications, since these objects are located within the errors across the fundamental blue edge. Due to the well-known correlation between the pulsation periods and metallicity we also tested whether the metal content plays any role in the mode identification. We split the SX Phe in GGCs in two metallicity bins i.e.  $[Fe/H] \leq -1.6$  and  $[Fe/H] > -1.6$ . Unfortunately, the distribution of SX Phe in the  $M_V - \log P$  plane does not show any significant change.

To overcome the problem it has been suggested by Alcock et al. (2000) and McNamara (2000) to account for the asymmetry of the light curve, and indeed fundamental pulsators should present larger amplitudes and more asymmetric light curves when compared with first overtone ones. Current data for SX Phe in  $\omega$  Cen seem to support this trend, but the observational scenario is still controversial. In fact, McNamara found that at least one, and maybe two, of the FOs in Carina present asymmetric light curves. A similar conclusion was also reached by Mateo, Hurley-Keller, & Nemeč (1998) and by Poretti (1999) on the basis of empirical data as well as by Bono et al. (1997) and by Templeton et al. (1998) according to nonlinear theoretical models.

Finally, we decided to check whether the secular period change  $-dP/(P dt) = \dot{P}/P$  can be adopted to overcome this thorny problem. This observable presents several advantages when compared with the previous ones: 1) it is the coupling of evolutionary and pulsational properties; 2) it is marginally affected by systematic errors. In particular, we estimated according to the pulsation relations given in §3.1 the variation of  $\dot{P}/P$  along three evolutionary tracks constructed by adopting the same chemical composition ( $Y=0.23$ ,  $Z=0.001$ ) but different stellar masses namely 1.2, 1.28 and 1.4  $M_{\odot}$ . Figure 6 shows the change of this parameter inside the instability strip for the first three radial modes as a function of the logarithmic period. Note that the effective temperature of the blue edge was fixed according to the models listed in Tables 1-3, while the red edge was located 1,500 K cooler than the previous one. The latter value is arbitrary and was chosen only to supply an upper limit to the width of the instability strip for each individual mode. Data plotted in this figure support the evidence that the secular period change can be adopted to identify the pulsation mode of SX Phe stars. In fact, the region in which this parameter attains similar values is, at fixed mode, quite narrow and located close to the blue edge. However, the secular period changes for the first three modes are quite similar for  $\dot{P}/P \leq 0.10$ . This finding suggests that the mode identification is more robust for SX Phe located in the middle or close to the red edge of the instability strip. Current empirical observations on secular period changes of SX Phe are quite scanty and only refer to metal-rich field objects (Breger & Pamyatnykh 1998).

The photometric databases collected by microlensing experiments on cluster SX Phe variables can supply useful constraints on the accuracy of such a parameter to identify the pulsation mode. However, it is worth noting that to detect and measure a phase drift in the time of maximum light due to evolutionary changes would require that the observations span a time interval of a few decades. In fact, by taking into account a first overtone pulsator with  $P=5,400$  s, the data plotted in the middle panel of Fig. 6 suggest that  $\dot{P} \approx 3.5 \times 10^{-14} s s^{-1}$ . Therefore according to Kepler et al. (2000) to detect a difference of a few seconds in the observed minus calculated times of maxima is necessary that the observations cover a time interval of  $\approx 10 - 20$  yr (see also Breger & Pamyatnykh 1998).

## 5. High overtone models

Together with the previous grid of models we also constructed several models along an evolutionary track at fixed stellar mass ( $M/M_{\odot}=1.2$ ) and chemical composition ( $Y=0.23^7$ ,  $Z=0.001$ ). The adopted temperature step is roughly 300 K, and the modal stability was estimated up to the sixth overtone. We adopted a different approach to construct these models, since we plan to perform the nonlinear analysis on these structures. Moreover, to investigate the dependence of linear observables on He content we also constructed an evolutionary track in which, immediately after the central H exhaustion, the He content of the envelope was artificially enhanced to  $Y=0.30$ . This evolutionary track is a crude representation of the aftermath of the collisional merging. We are aware that it was constructed by adopting severe over-simplifications, but they are only aimed at testing whether linear nonadiabatic observables do depend on He content. Figure 7 shows the two evolutionary tracks in the HR diagram together with the pulsation models (filled circles). The inner boundary for some of the hottest models was slightly moved toward the surface to maintain approximately constant the envelope mass across the strip. However in agreement with G98, we find that the period difference between canonical and shallower models is of the order of 0.0002 day and smaller than 0.0003 day for period ratios. Table 5 lists the input parameters, the periods and the pulsation constants for the two sets of models.

Data listed in this table show that the models constructed by adopting a higher He content present a different modal stability at hotter effective temperatures. In fact, among He-enhanced models the fundamental mode becomes unstable for temperature roughly

---

<sup>7</sup>The pulsational models distributed along the canonical track were constructed by adopting a He content slightly higher than the evolutionary one (0.24 against 0.23). This difference is motivated by homogeneity with previous calculations and also because it has a marginal effect on the pulsation behavior.

equal to 7,000 K, whereas for canonical models it becomes unstable close to 8,000 K. Canonical and He-enhanced models show at lower effective temperatures a similar behavior, and indeed for  $T_e \leq 7,300\text{K}$  higher overtones, as expected, become rapidly stable.

The evidence that at higher effective temperatures the He-enhanced models present a different modal stability when compared with the canonical ones is worth being investigated. In order to assess whether this difference is caused by the increase in the He content we performed a numerical experiment by constructing two models at fixed stellar mass ( $M/M_\odot=1.2$ ), luminosity ( $\log L/L_\odot=0.98$ ), effective temperature ( $T_e = 7,900\text{ K}$ ), and metal abundance ( $Z=0.001$ ) but different helium contents, namely  $Y=0.24$  and  $Y=0.30$ . Interestingly enough, we find that the pulsation properties of the two models are almost identical, and indeed the periods of the He-enhanced model are slightly longer ( $< 1\%$ ), while the total kinetic energy is larger by an amount which ranges from 15% for the second overtone to less than 2% for the sixth overtone. This finding suggests that at fixed input parameters an increase of 20% in the He content does not cause a substantial change in the pulsation characteristics.

As a consequence, the change in the modal stability of hot models is caused by evolutionary effects, and in particular by the increase in luminosity. Figure 8 shows the total works for the first six modes of the two pulsation models constructed by adopting the same mass value and metal content but different luminosities and He abundances (see labeled values). Data plotted in this figure show that the increase in the luminosity causes in He-enhanced models a decrease in the mean density, and in turn a systematic shift of both H and He driving regions toward the center. At the same time, the work curves show that the Z-bump, due to metals, plays a marginal role in the destabilization of higher overtones. In fact, the nonadiabatic region -i.e. the envelope region which drives these modes- moves toward the stellar surface, and therefore their properties are marginally affected by the innermost adiabatic regions.

On the other hand, the periods of He-enhanced model are approximately 20% longer than the canonical ones (see Table 5). Moreover we also find that the total kinetic energy of He-enhanced model is  $\approx 20\%$  smaller among lower modes and the difference becomes vanishing among higher overtones. This implies that SX Phe variables characterized by a large He content in the envelope should present larger pulsation destabilizations when compared with the canonical ones. These results, once confirmed by nonlinear, limiting cycle calculations, suggest that not only the period distribution but also the pulsation amplitudes inside the instability strip can be adopted to constrain the evolutionary history of SX Phe stars.

Finally, we decided to investigate whether the secular period change of both He-

enhanced and canonical models present a different behavior in the  $\dot{P}/P$  vs  $\log P$  plane. Figure 9 shows the secular period changes estimated along the two evolutionary tracks plotted in Figure 7. Note that the blue edges adopted to perform these calculations rely on the pulsation models listed in Table 5, while the red edges were arbitrarily fixed 1,500 K cooler than the previous ones. Interestingly enough, Figure 9 shows that at fixed period the He-enhanced models present  $\dot{P}/P$  values that are on average a factor of two larger than the canonical ones. Note that the sharp jump in the  $\dot{P}/P$  values of He-enhanced first and second overtone models is due to the fact that the He-enhanced track does not present, as for the canonical one, a steady increase in luminosity and effective temperature. These changes are spurious and caused by the adjustment of the physical structure of the envelope soon after the change of its chemical profile. However, the sharp change of  $\dot{P}/P$  values further strengthens the strong sensitivity of this parameter even to small variations in the physical parameters. This finding supports the evidence that accurate estimates of secular period changes can also be adopted to constrain the physical mechanisms which trigger the formation of BSs.

## 6. Summary and conclusions

We constructed several sets of linear, nonadiabatic pulsation models to investigate the modal stability of SX Phe variables. To account for the pulsation behavior of SX Phe in GGCs and in dwarf galaxies we adopted stellar masses ranging from 1.0 to 1.4  $M_{\odot}$  and two different metal contents, namely  $Z=0.0001$  and  $Z=0.001$ . For each selected mass value and chemical composition we constructed model sequences which cover a wide range of luminosities and effective temperatures.

Current theoretical scenario, implemented with the more metal-rich calculations performed by G98, suggests that the pulsation behavior of SX Phe stars are partially affected by metal content. In fact, we find that metal-poor models present when compared with metal-rich ones marginal changes both in the pulsation period and in the total work. However, it is worth mentioning that a decrease in the metal content from  $Z=0.006$  to  $Z=0.0001$  causes a shift of the blue edge for the first three modes toward hotter effective temperatures ranging from 300 to 500 K. At the same time, we find that at fixed input parameters the total kinetic energy decreases by a factor of 5 between fundamental and first overtone and by a factor of 2.5 between first and second overtones. This finding further supports the evidence suggested by G98 that SX Phe variables should be enthusiastic overtone pulsators, since a decrease in the total kinetic energy implies a decrease in the pulsational inertia of the envelope, and in turn an increase in the pulsation destabilization.



On the basis of both current theoretical models and models constructed by G98 we estimated the pulsational relations for the first three radial modes. Interestingly enough we find that the inclusion of a metallicity term substantially improves the accuracy of the analytical periods. In fact, we find that over the entire period range the difference between computed and estimated periods is within 0.005 dex. Moreover and even more important, we confirm the result recently brought out by PCD99 that the inclusion of a metallicity term in the PLC relation causes a decrease in the intrinsic scatter of the relation. At the same time, we performed a detailed comparison of our PLCZ relation with a similar theoretical relation derived by PCD99 and with the empirical relation given by McNamara (1997), we find that the discrepancy over the entire period range is smaller than 5%. This result supports the use of SX Phe variables as standard candles, once the pulsation mode has been properly identified.

In order to disentangle the long-standing problem of mode identification we performed a detailed comparison in the  $M_V$  vs  $\log P$  plane between the predicted blue edges for the three first radial modes and current available data for SX Phe in GGCs, in dwarf galaxies, and in the Galactic field. The distribution of SX Phe in the instability strip and current uncertainties on distance moduli do not allow us to properly identify the pulsation mode of these objects. The outcome is the same if we use the luminosity amplitude vs period diagram or the HR diagram. Bright, short-period, high-overtone pulsators as for V15 and V16 in 47 Tuc (G98) might provide better prospects for identification, however for these superior photometry from 1999 (Bruntt et al. 2000) provide a V15 period ratio that is now inconsistent with a simple high-overtone interpretation. For V16 the new data confirm the lower amplitude pulsation found earlier, but the longer period mode is not detectable in the new data suggesting significant amplitude changes have occurred. The high overtone mode identifications for 47 Tuc SX Phe stars have not been shown to be secure.

The difficulties in the mode identification can be explained if we assume that the instability strip of SX Phe is characterized by wide "OR regions" i.e. regions within which two or more modes are simultaneously excited. This plausible but qualitative argument is supported by the large number of mixed-mode pulsators found in 47 Tuc by G98. However, it is clear that we come to a deadlock and SX Phe together with Mira are the two groups of radial variables for which we still lack a straightforward method to single out the pulsation mode. Therefore it seems quite interesting that secular period changes can be adopted to single out the pulsation mode of cooler SX Phe variables. To properly attack the problem, not only new and accurate data for SX Phe stars in GGCs and in dwarf galaxies are necessary, but also a detailed set of full amplitude nonlinear pulsation models are needed which can supply useful insights into their pulsation properties.

Together with the previous calculation we also constructed two new sets of pulsation models along two evolutionary tracks characterized by the same stellar mass ( $1.2 M_{\odot}$ ) and metal content but different He contents, namely 0.24 and 0.30. To supply a crude but straightforward representation of a stellar collision the latter track was constructed by artificially enhancing, soon after the central H exhaustion, the He content of the envelope. Unlike, the previous sets of models we estimated for these models the first seven modes i.e. fundamental and six overtones. Interestingly enough we find that the increase in the He causes, as expected, an increase in the stellar luminosity, which in turn causes a significant change in the pulsation behavior of SX Phe. In fact, among the He-enhanced models the fundamental mode becomes unstable for effective temperatures close to 7,000 K, while the canonical ones at 8,000 K. Moreover, the He-enhanced models present pulsation periods and total kinetic energies that are approximately 20% longer and 20% smaller than the canonical ones. It is noteworthy that the secular period changes of He-enhanced models are, on average, a factor of two larger than the canonical ones.

This finding brings out the evidence that the pulsation behavior of SX Phe and in particular luminosity amplitudes, period distributions, the topology of the instability strip, and the secular period change can supply useful constraints on the evolutionary history of BSs, and in turn on the physical mechanisms which trigger their formation in GGCs and in dwarf galaxies.

One of us (PS) wish to acknowledge the Rome Astronomical Observatory for the warm hospitality during which this paper was written. We are grateful to an anonymous referee for his/her useful suggestions that served to improve the content of the paper. This research has made use of NASA's Astrophysics Data System Abstract Service and of SIMBAD database operated at CDS, Strasbourg, France. This work was supported by MURST -Cofin2000- under the scientific project: "Stellar Observables of Cosmological relevance".

## REFERENCES

- Ahumada, J., & Lapasset, E. 1995, *A&AS*, 109, 375
- Alcock, C. et al. 2000, *ApJ*, 536, 798
- Alexander, D. R., & Ferguson, J. W. 1994, *ApJ*, 437, 879
- Auriere, M., Lauzeral, C., Ortolani, S. 1990, *Nature*, 344, 638
- Bailyn, C. D. 1992, *ApJ*, 392, 519
- Bailyn, C. D. 1995, *ARA&A*, 33, 133
- Bailyn, C. D., & Pinsonneault, M. H. 1995, *ApJ*, 439, 705
- Benz, W., & Hills, J. G. 1992, *ApJ*, 389, 546
- Bono, G., Caputo, F., Cassisi, S., Castellani, V., Marconi, M. & Stellingwerf, R. F. 1997, *ApJ*, 477, 346 (B97)
- Bono, G., Caputo, F., Castellani, V., & Marconi, M. 1999b, *ApJ*, 512, 711
- Bono, G., Incerpi, R., & Marconi, M. 1996, *ApJ*, 467, L97
- Bono, G., & Marconi, M. 1999, in *IAU Symp. 190, New views of the Magellanic Clouds*, ed. Chu, Y.-H., Suntzeff, N.B., Hesser, J.E., & Bohlender, D.A. (San Francisco: ASP), 527
- Bono, G., Marconi, M. & Stellingwerf, R. F. 1999a, *ApJS*, 122, 167
- Bono, G., & Stellingwerf, R. F. 1994, *ApJS*, 93, 233
- Borissova, J., Catelan, M., Ferraro, F. R., Spassova, N., Buonanno, R., Iannicola, G., Richtler, T. & Sweigart, A. V. 1999, *A&A* 343, 813
- Breger, M., & Pamyatnykh, A&A, 1998, 332, 958
- Bruntt, H., et al. 2001, *A&A*, submitted
- Buonanno, R., Corsi, C. E., Buzzoni, A., Cacciari, C., Ferraro, F. R., Fusi Pecci, F. 1994, *A&A*, 290, 69
- Carretta, E., Gratton, R. G. 1997, *A&AS*, 121, 95
- Castelli, F., Gratton, R. G., & Kurucz, R. L. 1997a, *A&A*, 318, 841

- Castelli, F., Gratton, R. G., & Kurucz, R. L. 1997b, *A&A*, 324, 432
- Deutsch, E. W., Margon, B., & Anderson, S. F. 2000, *ApJ*, 530, L21
- Dinescu, D. I., Girard, T. M., van Altena, W. F., Yang, T. -G., & Lee, Y. -W. 1996, *AJ*, 111, 1205
- Edmonds, P. D., Gilliland, R. L., Guhathakurta, P., Petro, L. D., Saha, A., & Shara, M. M. 1996
- Fernie, J. D. 1992, *AJ*, 103, 1647
- Ferraro, F. R., Fusi Pecci, F., Bellazzini, M. 1995, *A&A*, 294, 80
- Ferraro, F. R., et al. 1997, *A&A*, 324, 915
- Ferraro, F. R., Paltrinieri, B., Rood, R. T., Dorman, B. 1999, *AJ*, 522, 983
- Groenewegen, M. A. T. 2000, *A&A*, astro-ph/0010298
- Gilliland, R. L., Bono, G., Edmonds, P. D., Caputo, F., Cassisi, S., Petro, L. D., Saha, A. & Shara, M. M. 1998, *ApJ*, 507, 818 (G98)
- Grillmair, C. J., et al. 1998, *AJ*, 115, 14
- Grindlay, J. E. 1999, in *Annapolis Workshop on Magnetic Cataclysmic Variables*, ed. Hellier, C. & Mukai, K. (San Francisco, ASP), 377
- Guarnieri, M. D., Ortolani, S., Montegriffo, P., Renzini, A., Barbuy, B., Bica, E., Moneti, A. 1998, *A&A*, 331, 70
- Harris, W. E. 1996, *AJ*, 112, 1487
- Hintz, E. G., Joner, M. D., McNamara, D. H., Nelson, K. A., Moody, J. W., & Kim, C. 1997a, *PASP*, 109, 15
- Hintz, E., Hintz, M. L., & Joner, M. D. 1997b, *PASP*, 109, 1073
- Hög, E. & Petersen, J. O. 1997, *A&A*, 323, 827
- Iglesias, C. A., & Rogers, F. J. 1996, *ApJ*, 464, 943
- Kaluzny, J. 1997, *A&AS*, 122, 1
- Kaluzny, J., Hilditch, R. W., Clement, C., & Rucinski, S. M. 1998, *MNRAS*, 296, 347

- Kaluzny, J., Krzeminski, W. 1993, MNRAS, 264, 785
- Kaluzny, J., Krzeminski, W., & Mazur, B. 1995, AJ, 110, 2206
- Kaluzny, J., Krzeminski, W., & Nalezyty, M. 1997, A&AS, 125, 337
- Kaluzny, J., Kubiak, M., Szymanski, M., Udalski, A., Krzeminski, W., Mateo, M. 1996, A&AS, 120, 139
- Kaluzny, J., Kubiak, M., Szymanski, M., Udalski, A., Krzeminski, W., Mateo, M., & Stanek, K. 1997, A&AS, 122, 471
- Kaluzny, J., Thompson, I., Krzeminski, W., & Pych, W. 1999, A&A, 350, 496
- Kepler, S. O., et al. 2000, ApJ, 534, L185
- Kholopov, P. N., et al. 1998, GCVS, 4th Edition
- Landsman, W., Bohlin, R. C., Neff, S. G., O'Connell, R. W., Roberts, M. S., & Smith, A. M., & Stecher, T. P. 1998, AJ, 116, 789
- Lopez De Coca, P., Rolland, A., Rodriguez, E. & Garrido, R. 1990, A&AS, 83, 51
- Mateo, M. 1998, ARA&A, 36, 435
- Mateo, M., Harris, H. C., Nemec, J., & Olszewski, E. W. 1990, AJ, 100, 469
- Mateo, M., Hurley-Keller, D., & Nemec, J. N. 1998, AJ, 115, 1856
- Mateo, M., Udalski, A., Szymanski, M., Kaluzny, J., Kubiak, M., Krzeminski, W. 1995, AJ, 109, 588
- Mazur, B., Kaluzny, J., & Krzeminski, W. 1999a, MNRAS, 306, 727
- Mazur, B., Krzeminski, W., & Kaluzny, J. 1999b, AcA, 49, 551
- McNamara, D. H. 1995, AJ, 109, 1751
- McNamara, D. H. Powell, J. M., & Joner, M. D. 1996, PASP, 108, 1098
- McNamara, D. H. 1997, PASP, 109, 1221
- McNamara, D. H. 2000, PASP, 112, 1096
- Mochejska, B. J., Kaluzny, J., & Thompson, I. 2000, astro-ph/0002341

- Monkiewicz, J., et al. 1999, *PASP*, 111, 139
- Nemec, J. M., Nemec-Linnell, A. F., & Lutz, T. E. 1994, 108, 222
- Nemec, J. M. & Mateo, M. 1990, in *Confrontation between stellar pulsation and evolution*, ed. Cacciari, C. & Clementini, G. (San Francisco: ASP), 64
- Nemec, J. M. & Park, N. 1996, in *The origins, evolution, and destinies of binary stars in clusters*, ed. Milone, E.F. & Mermilliod, J.-C. (San Francisco: ASP), 359
- Niss, B. 1981, *A&A*, 98, 415
- Ouellette, J. A., Pritchett, C. J. 1998, *AJ*, 115, 2539
- Petersen, J. O., & Christensen-Dalsgaard, J. 1996, *A&A*, 312, 463
- Petersen, J. O., & Christensen-Dalsgaard, J. 1999, *A&A*, 352, 547 (PCD99)
- Petersen, J. O., & Hög, E. 1998a, *A&A*, 331, 989
- Petersen, J. O., & Hög, E. 1998b, *MemSait*, 69, 59
- Piotto, G., Zoccali, M., King, I. R., Djorgovski, S. G., Sosin, C., Dorman, B., Rich, R. M., & Meylan, G. 1999, *AJ*, 117, 264
- Poretti, E. 1999, *A&A*, 343, 385
- Rodríguez, E., & López-González, M. J. 2000, *A&A*, 359, 957 (RLG00)
- Rodriguez, E., Lopez De Coca, P., Rolland, A. & Garrido, R. 1990, *RMxA&A* 20, 37
- Rodriguez, E., Rolland, A., Lopez de Coca, P., Garcia-Lobo, E., Sedano, J. L. 1992, *A&AS*, 93, 189
- Rubenstein, E. P., & Bailyn, C. D. 1996, *AJ*, 111, 260
- Sandquist, E. L., Bolte, M., Hernquist, L. 1997, *ApJ*, 477, 335 (SBH97)
- Saviane, I., Piotto, G., Fagotto, F., Zaggia, S., Capaccioli, M., & Aparicio, A. 1998, *A&A*, 333, 479
- Shara, M. M., Saffer, R. A., & Livio, M. 1997, *ApJ*, 489, L59
- Sigurdsson, S., Davies, M. B., & Bolte, M. 1994, *ApJ*, 431, L115
- Sills, A., Bailyn, C. D. 1999, *ApJ*, 513, 428

Templeton, M. R., Guzik, J. A., & McNamara, B. J. 1998, BAAS, 193, 6405

Thompson, I. B., Kaluzny, J., Pych, W., Krzeminski, W. 1999, AJ, 118

Walker, A. R., & Nemec, J. M. 1996, AJ, 112, 2026

Wehlau, A., Rucinski, S. M., Shi, J., Fahlman, G. G., & Thompson, I. 1996, IBVS, 4394, 1

Wilson, W. J. F., Milone, E. F., Fry, D. J. I., & van Leeuwen, J. 1998, PASP, 110, 433

Yan, L., & Reid, I. N. 1996, MNRAS, 279, 751

---

This preprint was prepared with the AAS L<sup>A</sup>T<sub>E</sub>X macros v4.0.

Fig. 1.— *Left panels:* Opacity (top) and adiabatic exponent (bottom) for three models centrally located in the instability strip and constructed by adopting fixed mass, luminosity, effective temperature, and He content but different metallicities (see labeled values). *Right panels:* total work curves per logarithmic temperature for the three models adopted in the left panels. The individual work curves were normalized using the same value of the total kinetic energy:  $KE(F)=3.92 \times 10^{44}$  erg for the fundamentals (top) and  $KE(FO)=5.55 \times 10^{43}$  erg for the first overtones (bottom). Fundamental and first overtone periods (d) are also plotted in the right panels.

Fig. 2.— Fractional difference between computed and analytical periods. The latter ones were estimated by adopting the pulsation relations which include the metallicity term. From top to bottom the panels refer to fundamental, first, and second overtone respectively. Models constructed by adopting different metal contents are plotted with different symbols.

Fig. 3.— Fractional difference in the bolometric magnitude at fixed metallicity ( $Z=0.006$ ) between different fundamental PLCZ relations as a function of logarithmic period. The fractional differences -i.e.  $(our - other)/our$ - were estimated between our PLCZ relation and the PLCZ relations based on theoretical models (triangles) and empirical data (circles) for HADS stars (McNamara 1997) derived by PCD99. See text for more details.

Fig. 4.— Comparison in the  $M_V - \log P$  plane between predicted blue edges for the first three radial modes and current data available in the literature for SX Phe in GGCs (top panel) and in the dwarf galaxies Carina and Sagittarius (bottom panel). See Table 4 for more details on empirical data. The error bar in the lower right corner is a plausible estimate of the uncertainties affecting current distance determinations.

Fig. 5.— Same as Figure 4, but for field SX Phe variables. Primary (fundamental) and secondary (first overtone) periods of double-mode variables are connected with a short-dashed line.

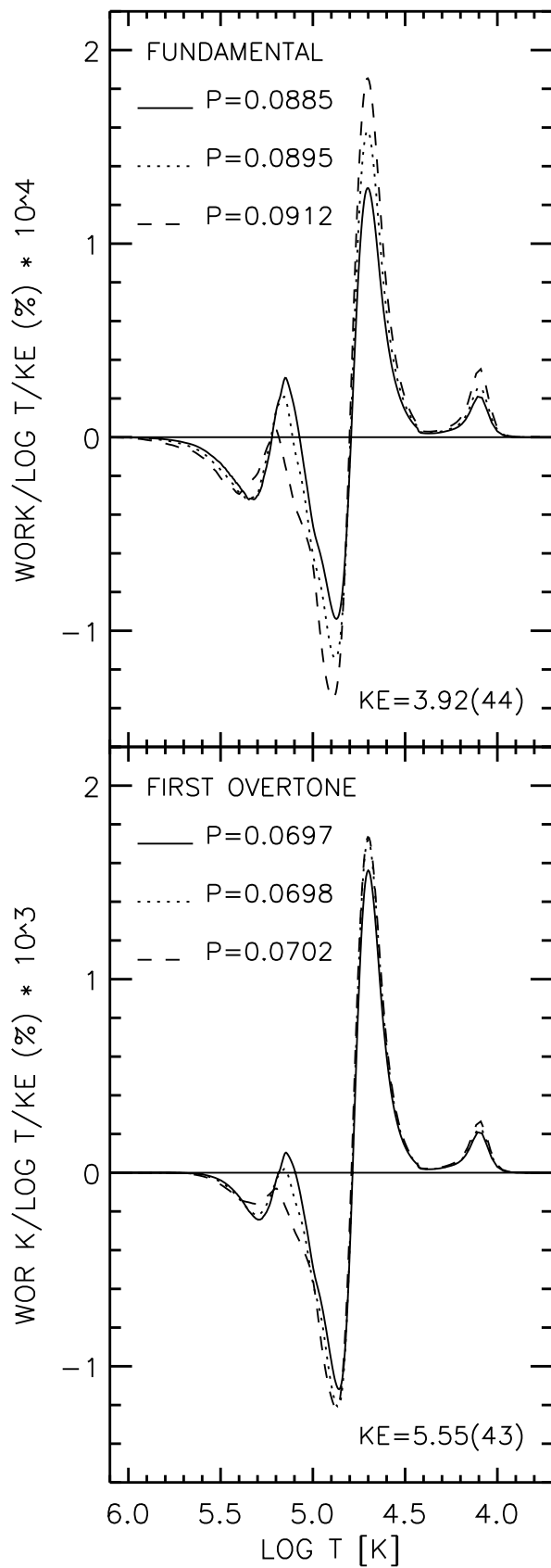
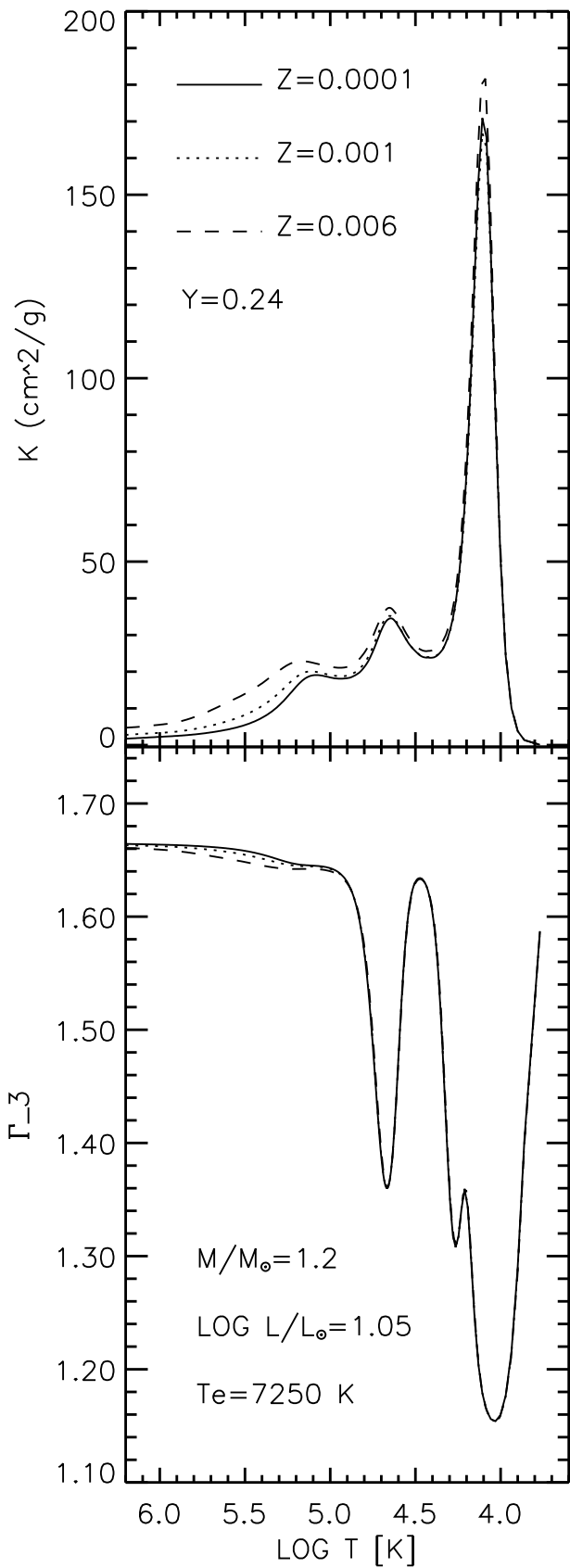
Fig. 6.— Secular period changes for the first three radial modes as a function of the pulsation period. The period changes were estimated along three different evolutionary tracks constructed by adopting the same composition ( $Y=0.23, Z=0.001$ ) but different stellar masses (see labeled values).

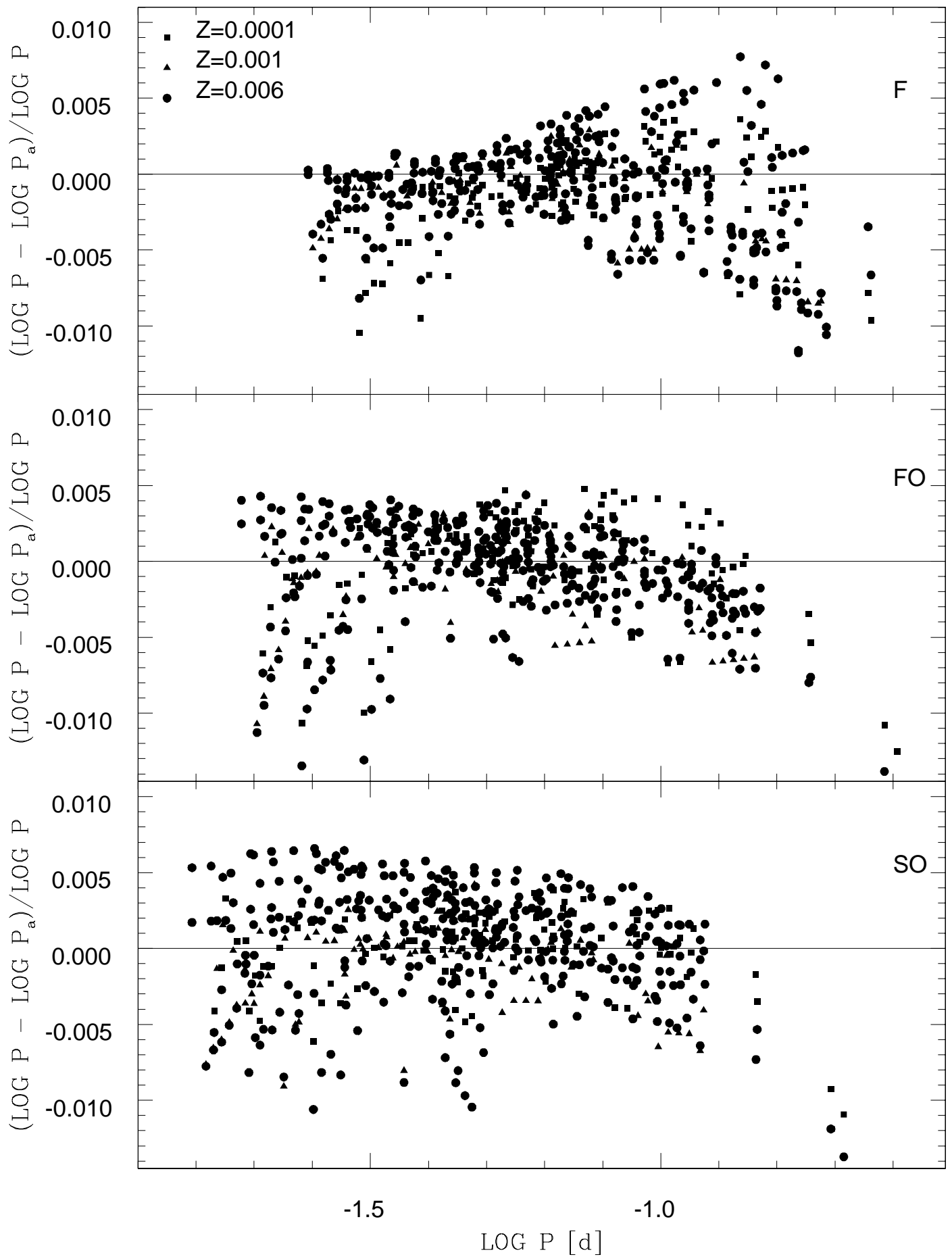
Fig. 7.— HR diagram showing the location of the pulsational models (open circles) constructed along the evolutionary tracks for  $M/M_\odot=1.2, Y=0.23$  and  $Z=0.001$  (solid line). The dashed line and the triangles refer to the evolutionary track whose He content in the envelope was artificially enhanced to  $Y=0.30$ . See text for more details.

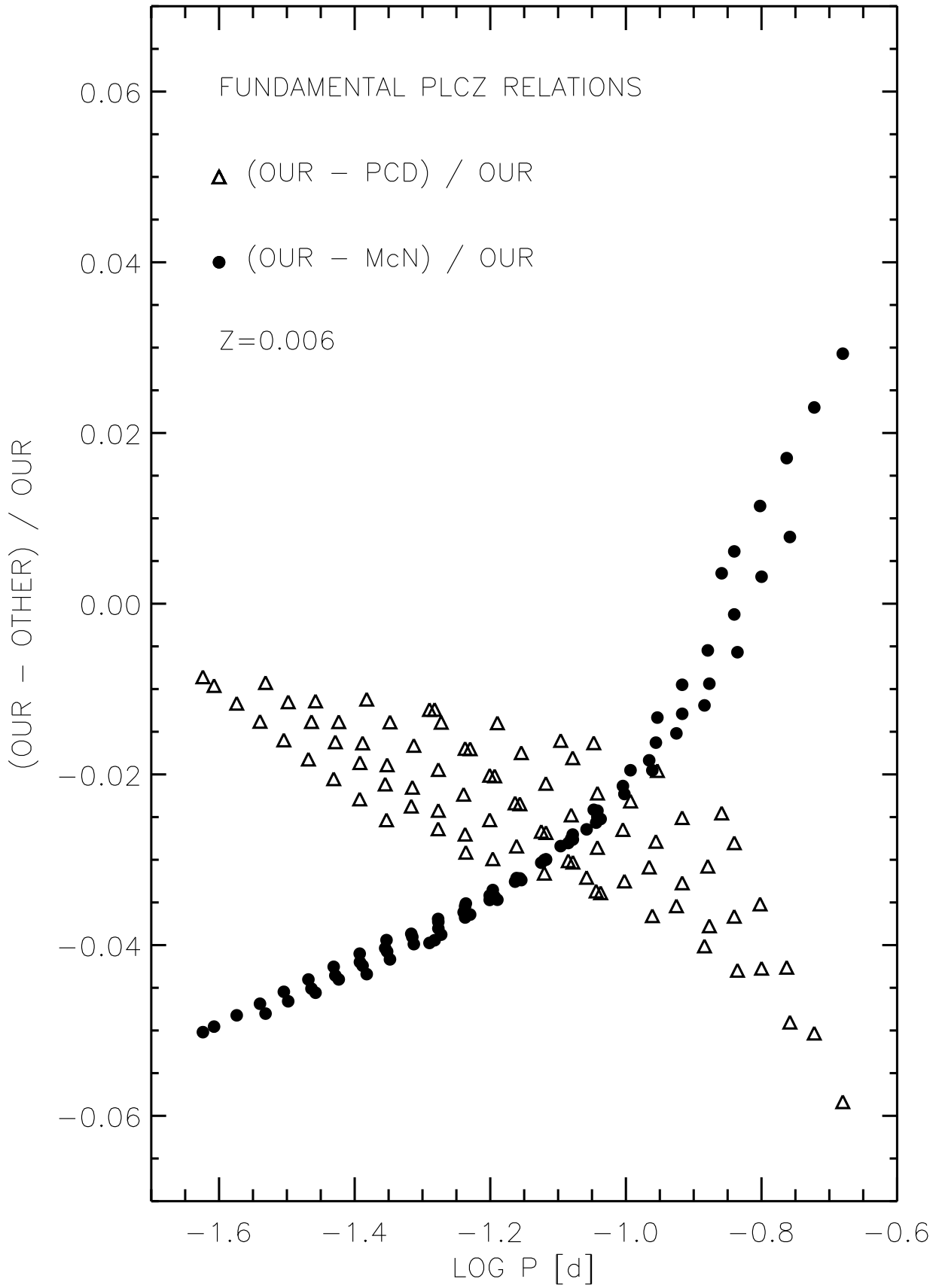


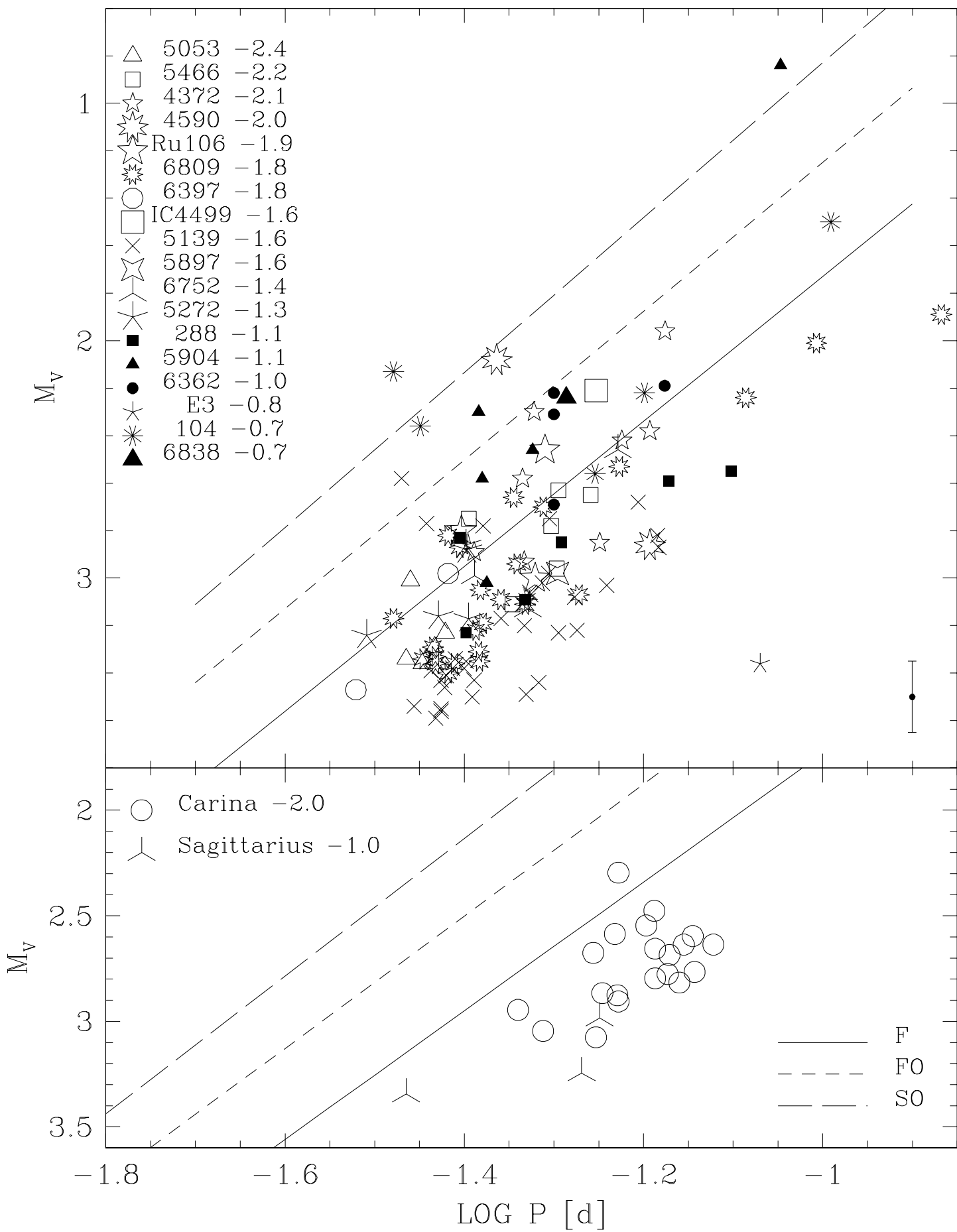
Fig. 8.— Total work curves for the first six radial modes as a function of the exterior mass. The two models were constructed by adopting the same stellar mass, effective temperature, and metal content (see labeled values), but different He contents and luminosities namely  $Y=0.24$ ,  $\log L/L_{\odot}=1.05$  (solid line) and  $Y=0.30$ ,  $\log L/L_{\odot}=1.18$  (dashed line). The individual work curves were normalized using the same value of the total kinetic energy (erg, lower right corner) and artificially enhanced by different factors (lower left corner). Linear periods (d) are also plotted.

Fig. 9.— Same as Figure 6, but for the evolutionary tracks plotted in Figure 7.









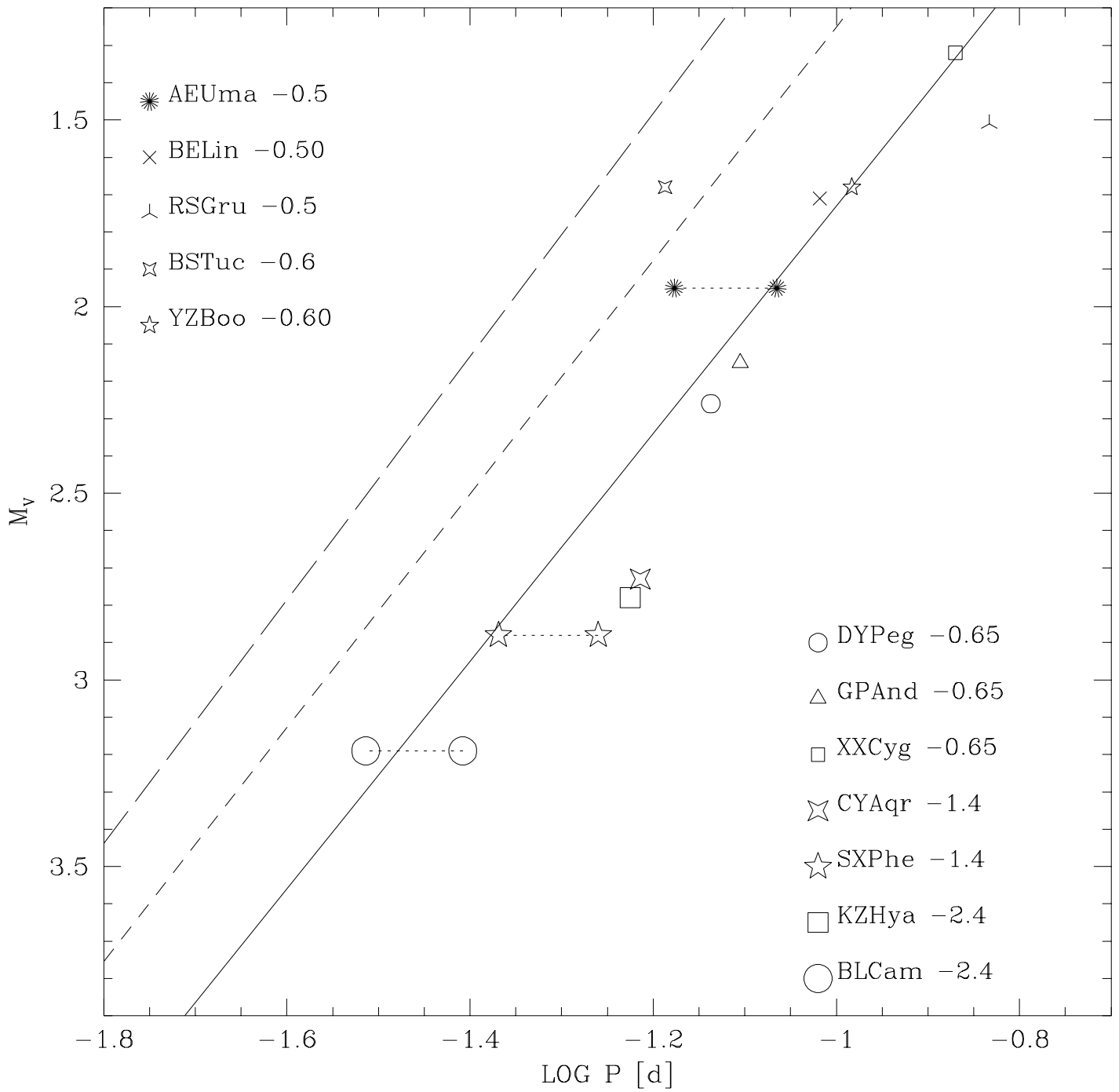




TABLE 1  
LINEAR NONADIABATIC FUNDAMENTAL MODELS

$L^a$	$T_e^b$	$R_{ph}^c$	$\Pi^d$	$Q^e$	$KE^f$	$W_t/KE^g$
(1)	(2)	(3)	(4)	(5)	(6)	(7)
$M/M_\odot = 1.4 \quad Z=0.0001$						
1.1	7800	1.3516(11)	7.2245(-2)	3.1588(-2)	1.312(45)	5.634(-8)
1.1	7700	1.3869(11)	7.5394(-2)	3.1713(-2)	1.309(45)	7.497(-7)
1.1	7600	1.4236(11)	7.8014(-2)	3.1553(-2)	1.127(45)	1.781(-6)
1.1	7000	1.6781(11)	9.9816(-2)	3.1544(-2)	7.330(44)	1.011(-5)
1.1	6500	1.9462(11)	1.2465(-1)	3.1540(-2)	5.055(44)	1.899(-5)
1.1	6300	2.0718(11)	1.3724(-1)	3.1617(-2)	4.496(44)	2.168(-5)
1.1	6100	2.2099(11)	1.5152(-1)	3.1686(-2)	3.957(44)	2.402(-5)
1.1	6000	2.2841(11)	1.5938(-1)	3.1718(-2)	3.688(44)	2.490(-5)
1.3	7500	1.8403(11)	1.1399(-1)	3.1369(-2)	4.518(44)	4.893(-6)
1.3	7000	2.1126(11)	1.4071(-1)	3.1481(-2)	3.175(44)	4.216(-5)
1.3	6500	2.4501(11)	1.7683(-1)	3.1676(-2)	2.306(44)	8.975(-5)
1.3	6000	2.8755(11)	2.2748(-1)	3.2052(-2)	1.807(44)	1.222(-4)
1.5	7300	2.4456(11)	1.7578(-1)	3.1577(-2)	1.928(44)	2.335(-5)
1.5	6700	2.9032(11)	2.2999(-1)	3.1941(-2)	1.322(44)	2.606(-4)
1.5	6100	3.5024(11)	3.1045(-1)	3.2539(-2)	1.020(44)	4.882(-4)
1.5	6000	3.6201(11)	3.2753(-1)	3.2668(-2)	9.901(43)	5.110(-4)
$M/M_\odot = 1.4 \quad Z=0.001$						
1.1	7600	1.4236(11)	7.8392(-2)	3.1706(-2)	7.942(44)	1.085(-6)
1.1	7100	1.6312(11)	9.6308(-2)	3.1759(-2)	5.787(44)	9.144(-6)
1.1	6600	1.8877(11)	1.2046(-1)	3.1908(-2)	4.383(44)	1.815(-5)
1.1	6300	2.0718(11)	1.3903(-1)	3.2030(-2)	3.742(44)	2.238(-5)
1.1	6000	2.2841(11)	1.6176(-1)	3.2193(-2)	3.214(44)	2.472(-5)
1.3	7400	1.8904(11)	1.2030(-1)	3.1798(-2)	3.434(44)	5.942(-6)
1.3	6900	2.1743(11)	1.4934(-1)	3.2001(-2)	2.567(44)	4.848(-5)
1.3	6400	2.5273(11)	1.8889(-1)	3.2299(-2)	2.007(44)	9.359(-5)
1.3	6000	2.8755(11)	2.3166(-1)	3.2641(-2)	1.717(44)	1.160(-4)
1.5	7200	2.5139(11)	1.8684(-1)	3.2204(-2)	1.654(44)	2.923(-5)
1.5	6700	2.9031(11)	2.3452(-1)	3.2573(-2)	1.279(44)	2.253(-4)
1.5	6400	3.1816(11)	2.7140(-1)	3.2855(-2)	1.128(44)	3.496(-4)
1.5	6000	3.6200(11)	3.3415(-1)	3.3331(-2)	1.005(44)	4.632(-4)
$M/M_\odot = 1.2 \quad Z=0.0001$						
0.7	8200	7.7147(10)	3.4230(-2)	3.2131(-2)	3.712(45)	4.623(-9)
0.7	8100	7.9063(10)	3.5446(-2)	3.2069(-2)	3.422(45)	5.561(-8)
0.7	8000	8.1052(10)	3.6739(-2)	3.2023(-2)	3.172(45)	1.157(-7)
0.7	7600	8.9809(10)	4.3032(-2)	3.2159(-2)	2.727(45)	3.836(-7)
0.7	6600	1.1909(11)	6.4812(-2)	3.1722(-2)	1.205(45)	1.597(-6)
0.7	6500	1.2278(11)	6.7897(-2)	3.1744(-2)	1.141(45)	1.675(-6)
0.7	6400	1.2664(11)	7.1291(-2)	3.1816(-2)	1.107(45)	1.696(-6)
0.7	6300	1.3070(11)	7.4362(-2)	3.1655(-2)	9.481(44)	1.919(-6)
0.9	8000	1.0205(11)	5.1191(-2)	3.1583(-2)	1.294(45)	1.832(-8)
0.9	7900	1.0465(11)	5.2934(-2)	3.1449(-2)	1.138(45)	4.052(-7)
0.9	7800	1.0735(11)	5.5123(-2)	3.1521(-2)	1.109(45)	7.885(-7)
0.9	6400	1.5946(11)	9.9559(-2)	3.1449(-2)	4.111(44)	1.073(-5)
0.9	6300	1.6456(11)	1.0438(-1)	3.1449(-2)	3.805(44)	1.141(-5)
0.9	6200	1.6991(11)	1.0977(-1)	3.1524(-2)	3.651(44)	1.156(-5)
1.1	7700	1.3869(11)	8.0254(-2)	3.1253(-2)	4.365(44)	2.111(-6)



TABLE 1—*Continued*

L <sup>a</sup>	T <sub>e</sub> <sup>b</sup>	R <sub>ph</sub> <sup>c</sup>	Π <sup>d</sup>	Q <sup>e</sup>	KE <sup>f</sup>	W <sub>t</sub> /KE <sup>g</sup>
(1)	(2)	(3)	(4)	(5)	(6)	(7)
1.1	7600	1.4236(11)	8.3426(-2)	3.1239(-2)	4.027(44)	4.834(-6)
1.1	7300	1.5430(11)	9.4292(-2)	3.1289(-2)	3.291(44)	1.509(-5)
1.1	7000	1.6781(11)	1.0705(-1)	3.1321(-2)	2.649(44)	2.864(-5)
1.1	6700	1.8318(11)	1.2247(-1)	3.1419(-2)	2.202(44)	4.229(-5)
1.1	6400	2.0075(11)	1.4110(-1)	3.1550(-2)	1.852(44)	5.430(-5)
1.1	6200	2.1391(11)	1.5577(-1)	3.1668(-2)	1.663(44)	6.036(-5)
1.1	6100	2.2099(11)	1.6390(-1)	3.1734(-2)	1.577(44)	6.252(-5)
1.1	6000	2.2841(11)	1.7272(-1)	3.1824(-2)	1.509(44)	6.330(-5)
			M/M <sub>⊙</sub> =1.2	Z=0.001		
0.6	8100	7.0472(10)	2.9713(-2)	3.1945(-2)	2.982(45)	2.752(-8)
0.6	7600	8.0049(10)	3.6014(-2)	3.1983(-2)	2.329(45)	2.516(-7)
0.6	7100	9.1721(10)	4.4089(-2)	3.1924(-2)	1.716(45)	5.399(-7)
0.6	6700	1.0300(11)	5.2270(-2)	3.1805(-2)	1.283(45)	7.804(-7)
0.6	6600	1.0614(11)	5.5018(-2)	3.2000(-2)	1.329(45)	7.450(-7)
0.6	6500	1.0944(11)	5.7314(-2)	3.1843(-2)	1.155(45)	8.377(-7)
0.6	6200	1.2028(11)	6.6324(-2)	3.1978(-2)	1.013(45)	8.032(-7)
0.6	6100	1.2426(11)	6.9438(-2)	3.1886(-2)	9.027(44)	8.023(-7)
0.7	8000	8.1052(10)	3.6564(-2)	3.1871(-2)	1.937(45)	6.717(-8)
0.7	7500	9.2219(10)	4.4221(-2)	3.1760(-2)	1.386(45)	6.736(-7)
0.7	7000	1.0586(11)	5.4261(-2)	3.1684(-2)	9.992(44)	1.457(-6)
0.7	6600	1.1909(11)	6.5023(-2)	3.1825(-2)	8.369(44)	1.851(-6)
0.7	6500	1.2278(11)	6.7853(-2)	3.1723(-2)	7.469(44)	2.047(-6)
0.7	6200	1.3495(11)	7.8310(-2)	3.1773(-2)	6.237(44)	2.137(-6)
0.7	6100	1.3941(11)	8.2418(-2)	3.1848(-2)	6.017(44)	2.030(-6)
0.9	7800	1.0735(11)	5.5252(-2)	3.1595(-2)	7.490(44)	4.369(-7)
0.9	7300	1.2256(11)	6.7477(-2)	3.1631(-2)	5.547(44)	4.100(-6)
0.9	6800	1.4125(11)	8.3682(-2)	3.1706(-2)	4.147(44)	8.438(-6)
0.9	6400	1.5946(11)	1.0075(-1)	3.1825(-2)	3.337(44)	1.106(-5)
1.1	7600	1.4236(11)	8.4437(-2)	3.1618(-2)	3.206(44)	2.292(-6)
1.1	7100	1.6312(11)	1.0399(-1)	3.1748(-2)	2.377(44)	2.264(-5)
1.1	6600	1.8877(11)	1.3038(-1)	3.1975(-2)	1.835(44)	4.518(-5)
1.1	6200	2.1391(11)	1.5857(-1)	3.2236(-2)	1.538(44)	5.723(-5)
			M/M <sub>⊙</sub> =1.0	Z=0.0001		
0.6	8300	6.7116(10)	2.9901(-2)	3.1574(-2)	1.605(45)	1.428(-8)
0.6	8200	6.8763(10)	3.1186(-2)	3.1755(-2)	1.679(45)	7.915(-8)
0.6	7600	8.0049(10)	3.8836(-2)	3.1484(-2)	1.038(45)	8.187(-7)
0.6	7100	9.1721(10)	4.7506(-2)	3.1401(-2)	7.391(44)	1.682(-6)
0.6	6700	1.0300(11)	5.6400(-2)	3.1327(-2)	5.518(44)	2.421(-6)
0.6	6600	1.0614(11)	5.8924(-2)	3.1286(-2)	5.049(44)	2.625(-6)
0.6	6400	1.1288(11)	6.4815(-2)	3.1379(-2)	4.601(44)	2.737(-6)
0.6	6300	1.1649(11)	6.7873(-2)	3.1343(-2)	4.194(44)	2.860(-6)
0.6	6200	1.2028(11)	7.1178(-2)	3.1329(-2)	3.859(44)	2.900(-6)
0.6	6100	1.2426(11)	7.4733(-2)	3.1327(-2)	3.567(44)	2.853(-6)
0.6	6000	1.2843(11)	7.8716(-2)	3.1400(-2)	3.417(44)	2.631(-6)
0.8	8100	8.8722(10)	4.4865(-2)	3.1171(-2)	5.871(44)	1.955(-8)
0.8	8000	9.0954(10)	4.6559(-2)	3.1165(-2)	5.501(44)	5.464(-7)
0.8	7400	1.0630(11)	5.8841(-2)	3.1172(-2)	3.723(44)	5.379(-6)

TABLE 1—*Continued*

$L^a$	$T_e^b$	$R_{ph}^c$	$\Pi^d$	$Q^e$	$KE^f$	$W_t/KE^g$
(1)	(2)	(3)	(4)	(5)	(6)	(7)
0.8	6800	1.2589(11)	7.5906(-2)	3.1203(-2)	2.498(44)	1.192(-5)
0.8	6500	1.3778(11)	8.7092(-2)	3.1269(-2)	2.071(44)	1.471(-5)
0.8	6400	1.4212(11)	9.1376(-2)	3.1316(-2)	1.963(44)	1.529(-5)
0.8	6300	1.4666(11)	9.5922(-2)	3.1357(-2)	1.851(44)	1.578(-5)
1.0	7800	1.2045(11)	7.0824(-2)	3.1106(-2)	2.235(44)	2.360(-6)
1.0	7600	1.2688(11)	7.6648(-2)	3.1141(-2)	1.959(44)	9.799(-6)
1.0	7300	1.3752(11)	8.6631(-2)	3.1191(-2)	1.595(44)	2.469(-5)
1.0	7000	1.4956(11)	9.8529(-2)	3.1278(-2)	1.317(44)	4.238(-5)
1.0	6700	1.6325(11)	1.1278(-1)	3.1392(-2)	1.102(44)	5.991(-5)
1.0	6400	1.7891(11)	1.3008(-1)	3.1560(-2)	9.408(43)	7.393(-5)
1.0	6300	1.8464(11)	1.3670(-1)	3.1635(-2)	8.979(43)	7.718(-5)
$M/M_\odot=1.0$ $Z=0.001$						
0.6	8100	7.0472(10)	3.2045(-2)	3.1451(-2)	8.851(44)	9.929(-8)
0.6	8000	7.2244(10)	3.3313(-2)	3.1499(-2)	8.578(44)	2.331(-7)
0.6	7600	8.0049(10)	3.8798(-2)	3.1454(-2)	6.693(44)	9.509(-7)
0.6	7100	9.1721(10)	4.7690(-2)	3.1523(-2)	5.167(44)	1.931(-6)
0.6	6700	1.0300(11)	5.6819(-2)	3.1560(-2)	4.114(44)	2.600(-6)
0.6	6600	1.0614(11)	5.9449(-2)	3.1564(-2)	3.863(44)	2.735(-6)
0.6	6500	1.0944(11)	6.2286(-2)	3.1590(-2)	3.661(44)	2.811(-6)
0.6	6400	1.1288(11)	6.5279(-2)	3.1603(-2)	3.443(44)	2.862(-6)
0.6	6300	1.1649(11)	6.8536(-2)	3.1649(-2)	3.281(44)	2.820(-6)
0.6	6200	1.2028(11)	7.1953(-2)	3.1670(-2)	3.086(44)	2.747(-6)
0.6	6100	1.2426(11)	7.5614(-2)	3.1696(-2)	2.905(44)	2.580(-6)
0.6	6000	1.2843(11)	7.9568(-2)	3.1740(-2)	2.752(44)	2.302(-6)
0.8	7900	9.3271(10)	4.8733(-2)	3.1412(-2)	3.815(44)	4.900(-7)
0.8	7600	1.0078(11)	5.4813(-2)	3.1457(-2)	3.226(44)	3.144(-6)
0.8	7100	1.1547(11)	6.7416(-2)	3.1545(-2)	2.430(44)	8.773(-6)
0.8	6600	1.3363(11)	8.4348(-2)	3.1703(-2)	1.874(44)	1.362(-5)
0.8	6500	1.3778(11)	8.8404(-2)	3.1740(-2)	1.778(44)	1.434(-5)
0.8	6400	1.4212(11)	9.2749(-2)	3.1786(-2)	1.692(44)	1.486(-5)
0.8	6300	1.4666(11)	9.7378(-2)	3.1833(-2)	1.607(44)	1.520(-5)
0.7	6100	1.3941(11)	9.0138(-2)	3.1796(-2)	2.041(44)	6.335(-6)
0.7	6000	1.4409(11)	9.4862(-2)	3.1844(-2)	1.933(44)	5.897(-6)

<sup>a</sup>Logarithmic luminosity (solar units). <sup>b</sup> Effective temperature (K). <sup>c</sup> Photospheric radius (cm). <sup>d</sup> Period (days). <sup>e</sup> Pulsation constant (days). <sup>f</sup> Total kinetic energy (ergs). <sup>g</sup> Total work normalized to the total kinetic energy.

TABLE 2  
 LINEAR NONADIABATIC FIRST OVERTONE MODELS

$L^a$	$T_e^b$	$\Pi_1/\Pi_0^c$	$\Pi^d$	$Q^e$	$KE^f$	$W_t/KE^g$
(1)	(2)	(3)	(4)	(5)	(6)	(7)
$M/M_\odot = 1.4 \quad Z=0.0001$						
1.1	8000	7.9346(-1)	5.3518(-2)	2.5246(-2)	2.008(44)	2.028(-6)
1.1	7900	7.9375(-1)	5.5557(-2)	2.5237(-2)	1.874(44)	8.261(-6)
1.1	7800	7.8784(-1)	5.6918(-2)	2.4886(-2)	1.492(44)	1.916(-5)
1.1	7700	7.9300(-1)	5.9787(-2)	2.5148(-2)	1.580(44)	2.421(-5)
1.1	7600	7.8858(-1)	6.1520(-2)	2.4882(-2)	1.311(44)	3.841(-5)
1.1	7000	7.9285(-1)	7.9139(-2)	2.5010(-2)	9.768(43)	9.852(-5)
1.1	6500	7.9356(-1)	9.8919(-2)	2.5029(-2)	7.695(43)	1.318(-4)
1.1	6300	7.9528(-1)	1.0914(-1)	2.5144(-2)	7.379(43)	1.260(-4)
1.1	6100	7.9564(-1)	1.2055(-1)	2.5211(-2)	6.981(43)	1.094(-4)
1.1	6000	7.9513(-1)	1.2673(-1)	2.5220(-2)	6.749(43)	9.521(-5)
1.3	7800	7.8769(-1)	7.9744(-2)	2.4685(-2)	7.118(43)	1.313(-5)
1.3	7700	7.8912(-1)	8.3127(-2)	2.4755(-2)	6.904(43)	5.082(-5)
1.3	7600	7.8881(-1)	8.6375(-2)	2.4733(-2)	6.436(43)	9.569(-5)
1.3	7500	7.8942(-1)	8.9987(-2)	2.4763(-2)	6.149(43)	1.414(-4)
1.3	7000	7.9180(-1)	1.1141(-1)	2.4927(-2)	5.058(43)	3.789(-4)
1.3	6500	7.9175(-1)	1.4000(-1)	2.5080(-2)	4.405(43)	5.350(-4)
1.3	6000	7.9004(-1)	1.7972(-1)	2.5322(-2)	4.166(43)	4.719(-4)
1.5	7600	7.8935(-1)	1.2249(-1)	2.4829(-2)	3.876(43)	4.386(-5)
1.5	7500	7.8948(-1)	1.2762(-1)	2.4862(-2)	3.716(43)	2.037(-4)
1.5	7400	7.8922(-1)	1.3297(-1)	2.4880(-2)	3.547(43)	3.779(-4)
1.5	7300	7.8946(-1)	1.3877(-1)	2.4929(-2)	3.433(43)	5.535(-4)
1.5	6700	7.8718(-1)	1.8104(-1)	2.5144(-2)	2.876(43)	1.606(-3)
1.5	6100	7.8085(-1)	2.4241(-1)	2.5408(-2)	2.696(43)	1.987(-3)
1.5	6000	7.7932(-1)	2.5525(-1)	2.5459(-2)	2.694(43)	1.934(-3)
$M/M_\odot = 1.4 \quad Z=0.001$						
1.1	7900	7.7733(-1)	5.4171(-2)	2.4608(-2)	1.168(44)	4.762(-6)
1.1	7800	7.7890(-1)	5.6461(-2)	2.4687(-2)	1.144(44)	1.424(-5)
1.1	7700	7.7813(-1)	5.8585(-2)	2.4643(-2)	1.061(44)	2.582(-5)
1.1	7600	7.7959(-1)	6.1114(-2)	2.4718(-2)	1.038(44)	3.608(-5)
1.1	7100	7.8092(-1)	7.5209(-2)	2.4801(-2)	8.355(43)	9.286(-5)
1.1	6600	7.8282(-1)	9.4298(-2)	2.4978(-2)	7.256(43)	1.234(-4)
1.1	6300	7.8283(-1)	1.0884(-1)	2.5074(-2)	6.715(43)	1.196(-4)
1.1	6000	7.8194(-1)	1.2649(-1)	2.5173(-2)	6.278(43)	8.547(-5)
1.3	7700	7.7962(-1)	8.3025(-2)	2.4724(-2)	6.112(43)	2.142(-5)
1.3	7600	7.8016(-1)	8.6497(-2)	2.4768(-2)	5.907(43)	6.509(-5)
1.3	7500	7.7975(-1)	8.9991(-2)	2.4764(-2)	5.607(43)	1.138(-4)
1.3	7400	7.8019(-1)	9.3856(-2)	2.4808(-2)	5.432(43)	1.614(-4)
1.3	6900	7.8015(-1)	1.1651(-1)	2.4965(-2)	4.634(43)	3.926(-4)
1.3	6400	7.7807(-1)	1.4697(-1)	2.5131(-2)	4.157(43)	5.180(-4)
1.3	6000	7.7480(-1)	1.7949(-1)	2.5290(-2)	3.933(43)	4.645(-4)
1.5	7500	7.7754(-1)	1.2787(-1)	2.4911(-2)	3.590(43)	1.088(-4)
1.5	7400	7.7701(-1)	1.3323(-1)	2.4932(-2)	3.444(43)	2.796(-4)
1.5	7300	7.7671(-1)	1.3899(-1)	2.4969(-2)	3.329(43)	4.564(-4)
1.5	7200	7.7606(-1)	1.4500(-1)	2.4993(-2)	3.204(43)	6.414(-4)
1.5	6700	7.7263(-1)	1.8120(-1)	2.5167(-2)	2.784(43)	1.515(-3)
1.5	6400	7.6959(-1)	2.0887(-1)	2.5285(-2)	2.638(43)	1.871(-3)

TABLE 2—*Continued*

$L^a$ (1)	$T_e^b$ (2)	$\Pi_1/\Pi_0^c$ (3)	$\Pi^d$ (4)	$Q^e$ (5)	$KE^f$ (6)	$W_t/KE^g$ (7)
1.5	6000	7.6480(-1)	2.5556(-1)	2.5491(-2)	2.560(43)	1.952(-3)
$M/M_\odot = 1.2 \quad Z = 0.0001$						
0.7	8400	7.9100(-1)	2.5363(-2)	2.5592(-2)	5.060(44)	2.903(-7)
0.7	8300	7.9026(-1)	2.6199(-2)	2.5502(-2)	4.616(44)	7.858(-7)
0.7	8200	7.8820(-1)	2.6980(-2)	2.5325(-2)	4.054(44)	1.453(-6)
0.7	8100	7.8772(-1)	2.7922(-2)	2.5262(-2)	3.725(44)	2.150(-6)
0.7	8000	7.8756(-1)	2.8934(-2)	2.5220(-2)	3.453(44)	2.907(-6)
0.7	7600	7.9478(-1)	3.4201(-2)	2.5559(-2)	3.149(44)	5.206(-6)
0.7	6600	7.9407(-1)	5.1465(-2)	2.5189(-2)	1.486(44)	1.231(-5)
0.7	6500	7.9576(-1)	5.4029(-2)	2.5260(-2)	1.443(44)	1.170(-5)
0.7	6400	7.9910(-1)	5.6968(-2)	2.5424(-2)	1.459(44)	1.046(-5)
0.7	6300	7.9478(-1)	5.9101(-2)	2.5159(-2)	1.223(44)	1.022(-5)
0.9	8200	7.8334(-1)	3.7155(-2)	2.4686(-2)	1.520(44)	2.138(-6)
0.9	8100	7.8745(-1)	3.8864(-2)	2.4888(-2)	1.573(44)	5.003(-6)
0.9	8000	7.8760(-1)	4.0318(-2)	2.4875(-2)	1.467(44)	8.807(-6)
0.9	7900	7.8393(-1)	4.1497(-2)	2.4654(-2)	1.238(44)	1.482(-5)
0.9	7800	7.8733(-1)	4.3400(-2)	2.4818(-2)	1.258(44)	1.800(-5)
0.9	6400	7.9323(-1)	7.8974(-2)	2.4947(-2)	6.072(43)	6.432(-5)
0.9	6300	7.9291(-1)	8.2761(-2)	2.4936(-2)	5.764(43)	6.050(-5)
0.9	6200	7.9526(-1)	8.7295(-2)	2.5070(-2)	5.815(43)	5.185(-5)
1.1	8000	7.8490D-01	5.6159D-02	2.4527D-02	6.277(43)	6.537(-6)
1.1	7900	7.8471D-01	5.8261D-02	2.4503D-02	5.829(43)	2.777(-5)
1.1	7800	7.8604D-01	6.0678D-02	2.4562D-02	5.632(43)	4.909(-5)
1.1	7700	7.8670D-01	6.3136D-02	2.4587D-02	5.359(43)	7.272(-5)
1.1	7600	7.8663D-01	6.5626D-02	2.4574D-02	5.019(43)	9.970(-5)
1.1	7300	7.8908D-01	7.4404D-02	2.4690D-02	4.467(43)	1.750(-4)
1.1	7000	7.8972D-01	8.4540D-02	2.4735D-02	3.928(43)	2.476(-4)
1.1	6700	7.9115D-01	9.6889D-02	2.4857D-02	3.632(43)	2.892(-4)
1.1	6400	7.9154D-01	1.1168D-01	2.4973D-02	3.396(43)	2.956(-4)
1.1	6200	7.9131D-01	1.2327D-01	2.5059D-02	3.282(43)	2.681(-4)
1.1	6100	7.9085D-01	1.2962D-01	2.5097D-02	3.229(43)	2.423(-4)
1.1	6000	7.9100D-01	1.3662D-01	2.5173D-02	3.228(43)	2.051(-4)
$M/M_\odot = 1.2 \quad Z = 0.001$						
0.6	8400	7.9497(-1)	2.1336(-2)	2.5584(-2)	5.801(44)	5.200(-8)
0.6	8300	7.9224(-1)	2.1989(-2)	2.5435(-2)	5.186(44)	3.148(-7)
0.6	8200	7.8759(-1)	2.2582(-2)	2.5189(-2)	4.427(44)	6.808(-7)
0.6	8100	7.8609(-1)	2.3357(-2)	2.5112(-2)	4.055(44)	1.051(-6)
0.6	7600	7.8770(-1)	2.8369(-2)	2.5193(-2)	3.203(44)	2.798(-6)
0.6	7100	7.8577(-1)	3.4644(-2)	2.5085(-2)	2.307(44)	4.594(-6)
0.6	6700	7.8149(-1)	4.0849(-2)	2.4855(-2)	1.647(44)	5.389(-6)
0.6	6600	7.8995(-1)	4.3461(-2)	2.5278(-2)	1.893(44)	4.351(-6)
0.6	6500	7.8331(-1)	4.4895(-2)	2.4943(-2)	1.528(44)	4.421(-6)
0.6	6200	7.8921(-1)	5.2343(-2)	2.5237(-2)	1.471(44)	1.273(-6)
0.7	8300	7.8139(-1)	2.5517(-2)	2.4839(-2)	2.825(44)	3.254(-7)
0.7	8200	7.9202(-1)	2.7013(-2)	2.5356(-2)	3.415(44)	7.146(-7)
0.7	8100	7.7870(-1)	2.7306(-2)	2.4705(-2)	2.363(44)	2.114(-6)
0.7	8000	7.8532(-1)	2.8715(-2)	2.5029(-2)	2.614(44)	2.516(-6)

TABLE 2—*Continued*

$L^a$	$T_e^b$	$\Pi_1/\Pi_0^c$	$\Pi^d$	$Q^e$	$KE^f$	$W_t/KE^g$
(1)	(2)	(3)	(4)	(5)	(6)	(7)
0.7	7500	7.8079(-1)	3.4527(-2)	2.4798(-2)	1.759(44)	8.016(-6)
0.7	7000	7.7852(-1)	4.2243(-2)	2.4667(-2)	1.256(44)	1.297(-5)
0.7	6600	7.8472(-1)	5.1024(-2)	2.4973(-2)	1.166(44)	1.164(-5)
0.7	6500	7.8050(-1)	5.2959(-2)	2.4760(-2)	1.003(44)	1.171(-5)
0.7	6200	7.8180(-1)	6.1222(-2)	2.4840(-2)	8.897(43)	4.880(-6)
0.7	6100	7.8423(-1)	6.4634(-2)	2.4976(-2)	8.968(43)	1.408(-6)
0.9	8100	7.7668(-1)	3.8321(-2)	2.4540(-2)	1.084(44)	1.825(-6)
0.9	8000	7.7692(-1)	3.9789(-2)	2.4548(-2)	1.028(44)	6.647(-6)
0.9	7900	7.7560(-1)	4.1201(-2)	2.4478(-2)	9.381(43)	1.254(-5)
0.9	7800	7.7723(-1)	4.2944(-2)	2.4557(-2)	9.208(43)	1.757(-5)
0.9	7300	7.7913(-1)	5.2573(-2)	2.4645(-2)	7.347(43)	4.582(-5)
0.9	6800	7.8085(-1)	6.5343(-2)	2.4758(-2)	6.104(43)	6.358(-5)
0.9	6400	7.8206(-1)	7.8792(-2)	2.4889(-2)	5.425(43)	5.865(-5)
1.1	7900	7.7765(-1)	5.8357(-2)	2.4543(-2)	5.148(43)	7.815(-6)
1.1	7800	7.7775(-1)	6.0655(-2)	2.4553(-2)	4.903(43)	3.167(-5)
1.1	7700	7.7841(-1)	6.3157(-2)	2.4595(-2)	4.737(43)	5.616(-5)
1.1	7600	7.7879(-1)	6.5759(-2)	2.4623(-2)	4.556(43)	8.199(-5)
1.1	7100	7.7963(-1)	8.1073(-2)	2.4752(-2)	3.811(43)	2.079(-4)
1.1	6600	7.7978(-1)	1.0167(-1)	2.4933(-2)	3.393(43)	2.751(-4)
1.1	6200	7.7846(-1)	1.2344(-1)	2.5095(-2)	3.167(43)	2.485(-4)
$M/M_\odot=1.0$ $Z=0.0001$						
0.6	8500	7.8058(-1)	2.1689(-2)	2.4599(-2)	1.861(44)	7.953(-7)
0.6	8400	7.8457(-1)	2.2656(-2)	2.4799(-2)	1.933(44)	1.442(-6)
0.6	8300	7.8419(-1)	2.3448(-2)	2.4760(-2)	1.789(44)	2.373(-6)
0.6	8200	7.9166(-1)	2.4688(-2)	2.5139(-2)	2.022(44)	2.652(-6)
0.6	7600	7.8710(-1)	3.0568(-2)	2.4781(-2)	1.193(44)	1.026(-5)
0.6	7100	7.8848(-1)	3.7457(-2)	2.4759(-2)	8.789(43)	1.592(-5)
0.6	6700	7.8888(-1)	4.4493(-2)	2.4713(-2)	6.776(43)	1.794(-5)
0.6	6600	7.8804(-1)	4.6435(-2)	2.4654(-2)	6.215(43)	1.773(-5)
0.6	6400	7.9258(-1)	5.1371(-2)	2.4870(-2)	6.113(43)	1.345(-5)
0.6	6300	7.9150(-1)	5.3721(-2)	2.4808(-2)	5.607(43)	1.087(-5)
0.6	6200	7.9116(-1)	5.6313(-2)	2.4786(-2)	5.252(43)	6.939(-6)
0.6	6100	7.9115(-1)	5.9125(-2)	2.4785(-2)	4.973(43)	1.692(-6)
0.8	8300	7.7943(-1)	3.2523(-2)	2.4312(-2)	7.033(43)	3.100(-6)
0.8	8200	7.8094(-1)	3.3815(-2)	2.4375(-2)	6.817(43)	8.181(-6)
0.8	8100	7.8026(-1)	3.5006(-2)	2.4322(-2)	6.236(43)	1.461(-5)
0.8	8000	7.8083(-1)	3.6355(-2)	2.4335(-2)	5.898(43)	2.107(-5)
0.8	7400	7.8525(-1)	4.6204(-2)	2.4478(-2)	4.430(43)	6.244(-5)
0.8	6800	7.8840(-1)	5.9844(-2)	2.4600(-2)	3.426(43)	8.975(-5)
0.8	6500	7.9003(-1)	6.8805(-2)	2.4703(-2)	3.106(43)	8.475(-5)
0.8	6400	7.9111(-1)	7.2288(-2)	2.4774(-2)	3.058(43)	7.733(-5)
0.8	6300	7.9174(-1)	7.5945(-2)	2.4826(-2)	2.991(43)	6.762(-5)
1.0	8100	7.8342(-1)	4.9508(-2)	2.4351(-2)	3.2223(43)	5.5962(-6)
1.0	8000	7.8408(-1)	5.1441(-2)	2.4376(-2)	3.0680(43)	3.2314(-5)
1.0	7900	7.8501(-1)	5.3511(-2)	2.4418(-2)	2.9451(43)	6.0444(-5)
1.0	7800	7.8532(-1)	5.5620(-2)	2.4428(-2)	2.7904(43)	9.1525(-5)
1.0	7600	7.8682(-1)	6.0308(-2)	2.4502(-2)	2.5757(43)	1.5453(-4)

TABLE 2—*Continued*

$L^a$	$T_e^b$	$\Pi_1/\Pi_0^c$	$\Pi^d$	$Q^e$	$KE^f$	$W_t/KE^g$
(1)	(2)	(3)	(4)	(5)	(6)	(7)
1.0	7300	7.8819(-1)	6.8282(-2)	2.4584(-2)	2.2868(43)	2.5000(-4)
1.0	7000	7.8951(-1)	7.7790(-2)	2.4695(-2)	2.0938(43)	3.2354(-4)
1.0	6700	7.8987(-1)	8.9078(-2)	2.4796(-2)	1.9413(43)	3.6528(-4)
1.0	6400	7.8973(-1)	1.0273D-01	2.4924(-2)	1.8412(43)	3.5300(-4)
1.0	6300	7.8974(-1)	1.0795D-01	2.4983(-2)	1.8249(43)	3.3084(-4)
$M/M_\odot=1.0$ $Z=0.001$						
0.6	8400	7.7435(-1)	2.2261(-2)	2.4367(-2)	1.256(44)	5.510(-7)
0.6	8300	7.7804(-1)	2.3237(-2)	2.4538(-2)	1.299(44)	1.501(-6)
0.6	8200	7.7732(-1)	2.4067(-2)	2.4507(-2)	1.206(44)	2.741(-6)
0.6	8100	7.7340(-1)	2.4783(-2)	2.4324(-2)	1.035(44)	4.546(-6)
0.6	8000	7.7576(-1)	2.5843(-2)	2.4436(-2)	1.037(44)	5.635(-6)
0.6	7600	7.7388(-1)	3.0025(-2)	2.4341(-2)	7.905(43)	1.210(-5)
0.6	7100	7.7726(-1)	3.7068(-2)	2.4501(-2)	6.546(43)	1.671(-5)
0.6	6700	7.7859(-1)	4.4239(-2)	2.4573(-2)	5.491(43)	1.633(-5)
0.6	6600	7.7856(-1)	4.6284(-2)	2.4574(-2)	5.222(43)	1.507(-5)
0.6	6500	7.7928(-1)	4.8539(-2)	2.4618(-2)	5.062(43)	1.289(-5)
0.6	6400	7.7941(-1)	5.0879(-2)	2.4632(-2)	4.848(43)	9.943(-6)
0.6	6300	7.8062(-1)	5.3501(-2)	2.4706(-2)	4.767(43)	6.039(-6)
0.6	6200	7.8073(-1)	5.6176(-2)	2.4726(-2)	4.583(43)	1.136(-6)
0.8	8200	7.7247(-1)	3.3634(-2)	2.4244(-2)	5.242(43)	2.250(-6)
0.8	8100	7.7333(-1)	3.4955(-2)	2.4286(-2)	5.056(43)	8.786(-6)
0.8	8000	7.7422(-1)	3.6345(-2)	2.4328(-2)	4.882(43)	1.562(-5)
0.8	7900	7.7396(-1)	3.7717(-2)	2.4312(-2)	4.588(43)	2.347(-5)
0.8	7600	7.7583(-1)	4.2526(-2)	2.4405(-2)	4.095(43)	4.571(-5)
0.8	7100	7.7812(-1)	5.2457(-2)	2.4546(-2)	3.444(43)	7.488(-5)
0.8	6600	7.8011(-1)	6.5801(-2)	2.4732(-2)	3.014(43)	7.819(-5)
0.8	6500	7.8018(-1)	6.8971(-2)	2.4763(-2)	2.932(43)	7.389(-5)
0.8	6400	7.8041(-1)	7.2382(-2)	2.4806(-2)	2.869(43)	6.667(-5)
0.8	6300	7.8038(-1)	7.5991(-2)	2.4841(-2)	2.801(43)	5.659(-5)

<sup>a</sup>Logarithmic luminosity (solar units). <sup>b</sup> Effective temperature (K). <sup>c</sup> Period ratio. <sup>d</sup> Period (days). <sup>e</sup> Pulsation constant (days). <sup>f</sup> Total kinetic energy (ergs). <sup>g</sup> Total work normalized to the total kinetic energy.

TABLE 3  
LINEAR NONADIABATIC SECOND OVERTONE MODELS

L <sup>a</sup>	T <sub>e</sub> <sup>b</sup>	Π <sub>2</sub> /Π <sub>0</sub> <sup>c</sup>	Π <sup>d</sup>	Q <sup>e</sup>	KE <sup>f</sup>	W <sub>t</sub> /KE <sup>g</sup>
(1)	(2)	(3)	(4)	(5)	(6)	(7)
<i>M/M</i> <sub>⊙</sub> = 1.4 Z=0.0001						
1.1	8200	6.4522(-1)	4.0102(-2)	2.0372(-2)	4.281(43)	1.586(-5)
1.1	8100	6.4973(-1)	4.2005(-2)	2.0567(-2)	4.414(43)	4.204(-5)
1.1	8000	6.5779(-1)	4.4368(-2)	2.0930(-2)	4.826(43)	5.947(-5)
1.1	7900	6.5822(-1)	4.6071(-2)	2.0928(-2)	4.617(43)	8.842(-5)
1.1	7800	6.5022(-1)	4.6975(-2)	2.0539(-2)	3.836(43)	1.426(-4)
1.1	7700	6.5716(-1)	4.9546(-2)	2.0840(-2)	4.123(43)	1.532(-4)
1.1	7600	6.5056(-1)	5.0753(-2)	2.0527(-2)	3.538(43)	2.096(-4)
1.1	7000	6.5364(-1)	6.5244(-2)	2.0619(-2)	3.072(43)	3.302(-4)
1.1	6500	6.5055(-1)	8.1093(-2)	2.0519(-2)	2.668(43)	3.016(-4)
1.1	6300	6.5187(-1)	8.9461(-2)	2.0610(-2)	2.668(43)	2.034(-4)
1.1	6100	6.5096(-1)	9.8631(-2)	2.0627(-2)	2.621(43)	4.595(-5)
1.3	8000	6.4540(-1)	6.0547(-2)	2.0221(-2)	2.316(43)	6.214(-5)
1.3	7900	6.4731(-1)	6.3122(-2)	2.0300(-2)	2.294(43)	1.861(-4)
1.3	7800	6.4571(-1)	6.5371(-2)	2.0235(-2)	2.146(43)	3.368(-4)
1.3	7700	6.4748(-1)	6.8206(-2)	2.0311(-2)	2.130(43)	4.587(-4)
1.3	7600	6.4599(-1)	7.0736(-2)	2.0255(-2)	2.009(43)	6.145(-4)
1.3	7500	6.4624(-1)	7.3665(-2)	2.0272(-2)	1.956(43)	7.465(-4)
1.3	7000	6.4651(-1)	9.0968(-2)	2.0353(-2)	1.773(43)	1.233(-3)
1.3	6500	6.4378(-1)	1.1384(-1)	2.0393(-2)	1.652(43)	1.314(-3)
1.3	6000	6.4109(-1)	1.4584(-1)	2.0548(-2)	1.682(43)	4.238(-4)
1.5	7800	6.4190(-1)	9.1957(-2)	2.0151(-2)	1.380(43)	3.243(-4)
1.5	7700	6.4114(-1)	9.5539(-2)	2.0141(-2)	1.317(43)	8.153(-4)
1.5	7600	6.4152(-1)	9.9549(-2)	2.0179(-2)	1.284(43)	1.282(-3)
1.5	7500	6.4133(-1)	1.0368(-1)	2.0197(-2)	1.245(43)	1.762(-3)
1.5	7400	6.4049(-1)	1.0791(-1)	2.0192(-2)	1.199(43)	2.259(-3)
1.5	7300	6.4070(-1)	1.1262(-1)	2.0231(-2)	1.178(43)	2.684(-3)
1.5	6700	6.3739(-1)	1.4659(-1)	2.0359(-2)	1.083(43)	4.465(-3)
1.5	6100	6.3186(-1)	1.9616(-1)	2.0560(-2)	1.135(43)	3.479(-3)
1.5	6000	6.3059(-1)	2.0654(-1)	2.0600(-2)	1.167(43)	2.800(-3)
<i>M/M</i> <sub>⊙</sub> = 1.4 Z=0.001						
1.1	8100	6.3748(-1)	4.1256(-2)	2.0201(-2)	3.759(43)	2.213(-5)
1.1	8000	6.3454(-1)	4.2574(-2)	2.0084(-2)	3.420(43)	6.310(-5)
1.1	7900	6.3465(-1)	4.4228(-2)	2.0091(-2)	3.295(43)	1.011(-4)
1.1	7800	6.3687(-1)	4.6166(-2)	2.0185(-2)	3.304(43)	1.324(-4)
1.1	7700	6.3459(-1)	4.7778(-2)	2.0097(-2)	3.062(43)	1.777(-4)
1.1	7600	6.3659(-1)	4.9904(-2)	2.0184(-2)	3.070(43)	2.048(-4)
1.1	7100	6.3536(-1)	6.1190(-2)	2.0178(-2)	2.641(43)	3.304(-4)
1.1	6600	6.3601(-1)	7.6614(-2)	2.0294(-2)	2.462(43)	3.109(-4)
1.1	6300	6.3497(-1)	8.8280(-2)	2.0338(-2)	2.363(43)	1.768(-4)
1.3	7900	6.3173(-1)	6.2208(-2)	2.0007(-2)	1.986(43)	1.422(-4)
1.3	7800	6.3240(-1)	6.4762(-2)	2.0047(-2)	1.942(43)	2.846(-4)
1.3	7700	6.3175(-1)	6.7278(-2)	2.0035(-2)	1.861(43)	4.407(-4)
1.3	7600	6.3234(-1)	7.0108(-2)	2.0075(-2)	1.826(43)	5.809(-4)
1.3	7500	6.3119(-1)	7.2846(-2)	2.0046(-2)	1.745(43)	7.394(-4)
1.3	7400	6.3167(-1)	7.5989(-2)	2.0086(-2)	1.720(43)	8.632(-4)
1.3	6900	6.3082(-1)	9.4205(-2)	2.0187(-2)	1.585(43)	1.291(-3)

TABLE 3—*Continued*

L <sup>a</sup>	T <sub>e</sub> <sup>b</sup>	Π <sub>2</sub> /Π <sub>0</sub> <sup>c</sup>	Π <sup>d</sup>	Q <sup>e</sup>	KE <sup>f</sup>	W <sub>t</sub> /KE <sup>g</sup>
(1)	(2)	(3)	(4)	(5)	(6)	(7)
1.3	6400	6.2808(-1)	1.1864(-1)	2.0287(-2)	1.510(43)	1.230(-3)
1.3	6000	6.2468(-1)	1.4472(-1)	2.0390(-2)	1.517(43)	3.861(-4)
1.5	7800	6.2805(-1)	9.1423(-2)	2.0035(-2)	1.265(43)	1.665(-4)
1.5	7700	6.2802(-1)	9.5165(-2)	2.0063(-2)	1.227(43)	6.515(-4)
1.5	7600	6.2741(-1)	9.9006(-2)	2.0070(-2)	1.181(43)	1.162(-3)
1.5	7500	6.2707(-1)	1.0312(-1)	2.0090(-2)	1.147(43)	1.665(-3)
1.5	7400	6.2639(-1)	1.0741(-1)	2.0099(-2)	1.111(43)	2.170(-3)
1.5	7300	6.2621(-1)	1.1206(-1)	2.0131(-2)	1.089(43)	2.628(-3)
1.5	7200	6.2549(-1)	1.1687(-1)	2.0143(-2)	1.062(43)	3.069(-3)
1.5	6700	6.2265(-1)	1.4603(-1)	2.0281(-2)	1.009(43)	4.403(-3)
1.5	6400	6.2018(-1)	1.6832(-1)	2.0376(-2)	1.014(43)	4.470(-3)
1.5	6000	6.1656(-1)	2.0603(-1)	2.0551(-2)	1.096(43)	2.794(-3)
<i>M</i> / <i>M</i> <sub>⊙</sub> = 1.2 <i>Z</i> = 0.0001						
0.7	8600	6.4585(-1)	1.9540(-2)	2.1159(-2)	1.043(44)	1.677(-6)
0.7	8500	6.4527(-1)	2.0031(-2)	2.0943(-2)	9.151(43)	4.846(-6)
0.7	8400	6.4547(-1)	2.0696(-2)	2.0883(-2)	8.499(43)	8.070(-6)
0.7	8300	6.4574(-1)	2.1407(-2)	2.0838(-2)	7.942(43)	1.155(-5)
0.7	8200	6.4499(-1)	2.2078(-2)	2.0724(-2)	7.236(43)	1.580(-5)
0.7	8100	6.4524(-1)	2.2871(-2)	2.0692(-2)	6.808(43)	1.970(-5)
0.7	8000	6.4570(-1)	2.3723(-2)	2.0678(-2)	6.455(43)	2.348(-5)
0.7	7600	6.5382(-1)	2.8136(-2)	2.1026(-2)	6.107(43)	3.185(-5)
0.7	6600	6.5717(-1)	4.2593(-2)	2.0847(-2)	3.940(43)	2.446(-5)
0.7	6500	6.5917(-1)	4.4755(-2)	2.0924(-2)	3.920(43)	1.601(-5)
0.7	6400	6.6314(-1)	4.7276(-2)	2.1098(-2)	4.023(43)	6.953(-6)
0.9	8400	6.4654(-1)	2.8588(-2)	2.0418(-2)	3.915(43)	7.823(-6)
0.9	8300	6.5338(-1)	3.0067(-2)	2.0717(-2)	4.210(43)	1.899(-5)
0.9	8200	6.4610(-1)	3.0645(-2)	2.0361(-2)	3.479(43)	4.213(-5)
0.9	8100	6.5161(-1)	3.2160(-2)	2.0595(-2)	3.657(43)	5.273(-5)
0.9	8000	6.5183(-1)	3.3368(-2)	2.0587(-2)	3.488(43)	6.967(-5)
0.9	7900	6.4657(-1)	3.4226(-2)	2.0334(-2)	3.021(43)	9.757(-5)
0.9	7800	6.5128(-1)	3.5901(-2)	2.0529(-2)	3.140(43)	1.051(-4)
0.9	6400	6.5190(-1)	6.4903(-2)	2.0502(-2)	2.095(43)	7.574(-5)
0.9	6300	6.5030(-1)	6.7875(-2)	2.0451(-2)	2.021(43)	2.618(-5)
1.1	8200	6.4321(-1)	4.2709(-2)	2.0087(-2)	1.868(43)	2.961(-5)
1.1	8100	6.4359(-1)	4.4334(-2)	2.0097(-2)	1.798(43)	1.055(-4)
1.1	8000	6.4527(-1)	4.6169(-2)	2.0164(-2)	1.775(43)	1.766(-4)
1.1	7900	6.4409(-1)	4.7821(-2)	2.0112(-2)	1.670(43)	2.625(-4)
1.1	7800	6.4566(-1)	4.9841(-2)	2.0176(-2)	1.653(43)	3.306(-4)
1.1	7700	6.4599(-1)	5.1843(-2)	2.0189(-2)	1.605(43)	4.035(-4)
1.1	7600	6.4491(-1)	5.3803(-2)	2.0146(-2)	1.526(43)	4.846(-4)
1.1	7300	6.4664(-1)	6.0973(-2)	2.0233(-2)	1.455(43)	6.374(-4)
1.1	7000	6.4499(-1)	6.9047(-2)	2.0202(-2)	1.347(43)	7.390(-4)
1.1	6700	6.4517(-1)	7.9012(-2)	2.0271(-2)	1.308(43)	7.182(-4)
1.1	6400	6.4406(-1)	9.0873(-2)	2.0320(-2)	1.270(43)	5.291(-4)
1.1	6200	6.4293(-1)	1.0015(-1)	2.0361(-2)	1.262(43)	2.460(-4)
1.1	6100	6.4194(-1)	1.0521(-1)	2.0371(-2)	1.259(43)	4.640(-5)
<i>M</i> / <i>M</i> <sub>⊙</sub> = 1.2 <i>Z</i> = 0.001						



TABLE 3—*Continued*

$L^a$	$T_e^b$	$\Pi_2/\Pi_0^c$	$\Pi^d$	$Q^e$	$KE^f$	$W_t/KE^g$
(1)	(2)	(3)	(4)	(5)	(6)	(7)
0.6	8600	6.5470(-1)	1.6481(-2)	2.1207(-2)	1.242(44)	2.790(-7)
0.6	8500	6.5395(-1)	1.6991(-2)	2.1110(-2)	1.152(44)	1.604(-6)
0.6	8400	6.5287(-1)	1.7523(-2)	2.1011(-2)	1.068(44)	3.093(-6)
0.6	8300	6.5175(-1)	1.8089(-2)	2.0925(-2)	9.949(43)	4.693(-6)
0.6	8200	6.4874(-1)	1.8601(-2)	2.0748(-2)	8.986(43)	6.660(-6)
0.6	8100	6.4796(-1)	1.9253(-2)	2.0699(-2)	8.478(43)	8.348(-6)
0.6	7600	6.5188(-1)	2.3477(-2)	2.0849(-2)	7.350(43)	1.358(-5)
0.6	7100	6.5100(-1)	2.8702(-2)	2.0783(-2)	5.990(43)	1.473(-5)
0.6	6700	6.4408(-1)	3.3666(-2)	2.0485(-2)	4.649(43)	5.944(-6)
0.6	6600	6.5625(-1)	3.6105(-2)	2.1000(-2)	5.415(43)	3.316(-6)
0.7	8500	6.4839(-1)	1.9749(-2)	2.0648(-2)	7.425(43)	1.212(-6)
0.7	8400	6.4707(-1)	2.0401(-2)	2.0585(-2)	6.951(43)	4.644(-6)
0.7	8300	6.4602(-1)	2.1096(-2)	2.0535(-2)	6.540(43)	8.323(-6)
0.7	8200	6.5775(-1)	2.2434(-2)	2.1058(-2)	7.540(43)	9.116(-6)
0.7	8100	6.4289(-1)	2.2544(-2)	2.0396(-2)	5.707(43)	1.659(-5)
0.7	8000	6.5155(-1)	2.3823(-2)	2.0766(-2)	6.311(43)	1.706(-5)
0.7	7500	6.4549(-1)	2.8544(-2)	2.0501(-2)	4.757(43)	3.227(-5)
0.7	7000	6.3922(-1)	3.4685(-2)	2.0253(-2)	3.621(43)	3.512(-5)
0.7	6600	6.4741(-1)	4.2097(-2)	2.0604(-2)	3.668(43)	1.219(-5)
0.9	8300	6.3333(-1)	2.8977(-2)	1.9965(-2)	2.981(43)	1.155(-5)
0.9	8200	6.3546(-1)	3.0181(-2)	2.0053(-2)	2.975(43)	2.895(-5)
0.9	8100	6.3852(-1)	3.1504(-2)	2.0175(-2)	3.022(43)	4.436(-5)
0.9	8000	6.3825(-1)	3.2687(-2)	2.0166(-2)	2.892(43)	6.319(-5)
0.9	7900	6.3484(-1)	3.3723(-2)	2.0035(-2)	2.618(43)	8.799(-5)
0.9	7800	6.3725(-1)	3.5210(-2)	2.0134(-2)	2.640(43)	1.011(-4)
0.9	7300	6.3666(-1)	4.2960(-2)	2.0138(-2)	2.249(43)	1.635(-4)
0.9	6800	6.3579(-1)	5.3204(-2)	2.0159(-2)	1.980(43)	1.575(-4)
0.9	6400	6.3536(-1)	6.4013(-2)	2.0220(-2)	1.849(43)	4.362(-5)
1.1	8100	6.3068(-1)	4.3855(-2)	1.9880(-2)	1.599(43)	6.236(-5)
1.1	8000	6.3086(-1)	4.5554(-2)	1.9895(-2)	1.547(43)	1.449(-4)
1.1	7900	6.3155(-1)	4.7394(-2)	1.9932(-2)	1.513(43)	2.247(-4)
1.1	7800	6.3107(-1)	4.9216(-2)	1.9923(-2)	1.453(43)	3.111(-4)
1.1	7700	6.3171(-1)	5.1254(-2)	1.9960(-2)	1.428(43)	3.859(-4)
1.1	7600	6.3182(-1)	5.3349(-2)	1.9977(-2)	1.393(43)	4.593(-4)
1.1	7100	6.3099(-1)	6.5616(-2)	2.0033(-2)	1.253(43)	7.004(-4)
1.1	6600	6.3025(-1)	8.2174(-2)	2.0152(-2)	1.190(43)	6.541(-4)
1.1	6200	6.2842(-1)	9.9648(-2)	2.0258(-2)	1.167(43)	2.038(-4)
				$M/M_\odot = 1.0$	$Z = 0.0001$	
0.6	8700	6.5064(-1)	1.7026(-2)	2.0706(-2)	5.014(43)	2.586(-6)
0.6	8600	6.4917(-1)	1.7542(-2)	2.0606(-2)	4.575(43)	6.635(-6)
0.6	8500	6.4169(-1)	1.7830(-2)	2.0223(-2)	3.695(43)	1.342(-5)
0.6	8400	6.4671(-1)	1.8675(-2)	2.0442(-2)	3.868(43)	1.623(-5)
0.6	8300	6.4661(-1)	1.9334(-2)	2.0416(-2)	3.648(43)	2.112(-5)
0.6	8200	6.5521(-1)	2.0433(-2)	2.0806(-2)	4.077(43)	2.136(-5)
0.6	7600	6.5180(-1)	2.5313(-2)	2.0521(-2)	2.820(43)	4.640(-5)
0.6	7100	6.5335(-1)	3.1038(-2)	2.0516(-2)	2.340(43)	4.965(-5)
0.6	6700	6.5203(-1)	3.6774(-2)	2.0426(-2)	1.979(43)	2.670(-5)

TABLE 3—Continued

$L^a$	$T_e^b$	$\Pi_2/\Pi_0^c$	$\Pi^d$	$Q^e$	$KE^f$	$W_t/KE^g$
(1)	(2)	(3)	(4)	(5)	(6)	(7)
0.6	6600	6.4984(-1)	3.8291(-2)	2.0331(-2)	1.852(43)	1.242(-5)
0.8	8500	6.4355(-1)	2.5052(-2)	2.0113(-2)	1.957(43)	1.004(-5)
0.8	8400	6.4138(-1)	2.5826(-2)	2.0012(-2)	1.784(43)	3.439(-5)
0.8	8300	6.4175(-1)	2.6778(-2)	2.0017(-2)	1.711(43)	5.793(-5)
0.8	8200	6.4387(-1)	2.7880(-2)	2.0097(-2)	1.698(43)	7.837(-5)
0.8	8100	6.4224(-1)	2.8814(-2)	2.0019(-2)	1.574(43)	1.064(-4)
0.8	8000	6.4268(-1)	2.9923(-2)	2.0029(-2)	1.520(43)	1.295(-4)
0.8	7400	6.4616(-1)	3.8021(-2)	2.0142(-2)	1.313(43)	2.185(-4)
0.8	6800	6.4597(-1)	4.9033(-2)	2.0156(-2)	1.136(43)	1.945(-4)
0.8	6500	6.4587(-1)	5.6250(-2)	2.0196(-2)	1.084(43)	8.079(-5)
0.8	6400	6.4695(-1)	5.9116(-2)	2.0260(-2)	1.093(43)	2.117(-5)
1.0	8300	6.4135(-1)	3.7661(-2)	1.9930(-2)	9.996(42)	2.958(-4)
1.0	8200	6.4227(-1)	3.9128(-2)	1.9967(-2)	9.747(42)	1.218(-4)
1.0	8100	6.4188(-1)	4.0563(-2)	1.9951(-2)	9.304(42)	2.219(-4)
1.0	8000	6.4219(-1)	4.2132(-2)	1.9965(-2)	9.013(42)	3.188(-4)
1.0	7900	6.4302(-1)	4.3832(-2)	2.0001(-2)	8.833(42)	4.083(-4)
1.0	7800	6.4264(-1)	4.5514(-2)	1.9990(-2)	8.501(42)	5.036(-4)
1.0	7600	6.4359(-1)	4.9330(-2)	2.0042(-2)	8.181(42)	6.550(-4)
1.0	7300	6.4334(-1)	5.5733(-2)	2.0066(-2)	7.686(42)	8.179(-4)
1.0	7000	6.4331(-1)	6.3385(-2)	2.0122(-2)	7.410(42)	8.680(-4)
1.0	6700	6.4201(-1)	7.2403(-2)	2.0154(-2)	7.111(42)	7.998(-4)
1.0	6400	6.4069(-1)	8.3342(-2)	2.0220(-2)	6.975(42)	4.739(-4)
1.0	6300	6.4062(-1)	8.7570(-2)	2.0266(-2)	7.022(42)	2.856(-4)
$M/M_\odot=1.0$ $Z=0.001$						
0.6	8600	6.4274(-1)	1.7236(-2)	2.0246(-2)	3.652(43)	1.821(-6)
0.6	8500	6.3603(-1)	1.7622(-2)	1.9986(-2)	3.105(43)	7.763(-6)
0.6	8400	6.3944(-1)	1.8383(-2)	2.0122(-2)	3.172(43)	1.180(-5)
0.6	8300	6.4568(-1)	1.9284(-2)	2.0364(-2)	3.399(43)	1.442(-5)
0.6	8200	6.4433(-1)	1.9949(-2)	2.0314(-2)	3.195(43)	1.931(-5)
0.6	8100	6.3698(-1)	2.0412(-2)	2.0033(-2)	2.699(43)	2.741(-5)
0.6	8000	6.4097(-1)	2.1353(-2)	2.0190(-2)	2.795(43)	2.939(-5)
0.6	7600	6.3510(-1)	2.4641(-2)	1.9976(-2)	2.193(43)	4.487(-5)
0.6	7100	6.3761(-1)	3.0408(-2)	2.0099(-2)	1.960(43)	4.083(-5)
0.6	6700	6.3625(-1)	3.6151(-2)	2.0080(-2)	1.708(43)	8.652(-6)
0.8	8400	6.3079(-1)	2.5549(-2)	1.9797(-2)	1.567(43)	1.323(-5)
0.8	8300	6.3085(-1)	2.6492(-2)	1.9803(-2)	1.507(43)	3.812(-5)
0.8	8200	6.3000(-1)	2.7431(-2)	1.9773(-2)	1.427(43)	6.492(-5)
0.8	8100	6.3089(-1)	2.8516(-2)	1.9812(-2)	1.399(43)	8.853(-5)
0.8	8000	6.3183(-1)	2.9661(-2)	1.9854(-2)	1.375(43)	1.106(-4)
0.8	7900	6.3040(-1)	3.0721(-2)	1.9802(-2)	1.294(43)	1.376(-4)
0.8	7600	6.3149(-1)	3.4614(-2)	1.9865(-2)	1.211(43)	1.876(-4)
0.8	7100	6.3184(-1)	4.2596(-2)	1.9931(-2)	1.091(43)	2.081(-4)
0.8	6600	6.3235(-1)	5.3338(-2)	2.0047(-2)	1.017(43)	9.691(-5)
0.8	6500	6.3196(-1)	5.5868(-2)	2.0058(-2)	1.000(43)	4.445(-5)

<sup>a</sup>Logarithmic luminosity (solar units). <sup>b</sup> Effective temperature (K). <sup>c</sup> Period ratio. <sup>d</sup> Period (days). <sup>e</sup> Pulsation constant (days). <sup>f</sup> Total kinetic energy (ergs). <sup>g</sup> Total work normalized to the total kinetic energy.

TABLE 4  
SX PHOENICIS STARS

Cluster Var.N.	logP	$\langle V \rangle$	$A_V$	mode	Refs
Galactic Globular Clusters					
<b>NGC 104 47 Tuc</b>					
V1	-1.199	15.59		F	G98
	-1.306			FO	
V2	-0.991	14.86		F	
	-1.104			FO	
V3	-1.254	15.93		nr <sup>a</sup>	
V14	-1.330	16.46		F	
	-1.442			FO	
	-1.534			SO	
V15	-1.479	15.50		P <sub>4</sub>	
	-1.540			P <sub>5</sub>	
V16	-1.449	15.73		P <sub>4</sub>	
	-1.504			P <sub>5</sub>	
<b>NGC 288</b>					
V4	-1.102	17.24	0.30		KKN97
V5	-1.292	17.54	0.46		
V6	-1.172	17.28	0.41		
V7	-1.398	17.92	0.06		
V8	-1.332	17.78	0.06		
V9	-1.405	17.52	0.05		
<b>E 3</b>					
V1	-1.07	17.48	0.4		MKT00
<b>NGC 4372</b>					
V2	-1.389	17.99	0.32		KK93
V6	-1.176	17.06	0.33		
V8	-1.193	17.48	0.64		
V14	-1.249	17.95	0.28		
V15	-1.333	18.03	0.26		
V18	-1.322	17.40	0.32		
V25	-1.224	17.52	0.32		
V29	-1.335	17.68	0.43		
<b>Ru 106</b>					
V3	-1.403	20.05	0.30		KKM95
V4	-1.310	19.71	0.14		
V11	-1.321	20.25	0.18		
<b>NGC 4590 M 68</b>					
V39	-1.193	18.05	0.71		W94
V48	-1.364	17.27	0.17		
<b>NGC 5053</b>					
NC7	-1.460	19.20	0.12		NM90
NC11	-1.447	19.55	0.25		
NC13	-1.433	19.48	0.13		
NC14	-1.421	19.42	0.08		
NC15	-1.465	19.53	0.13		
<b>NGC 5139 <math>\omega</math> Cen</b>					
OG1	-1.327	17.03	0.13		Kal96; Kal97; PH98

TABLE 4—*Continued*

Cluster Var.N.	logP	$\langle V \rangle$	$A_V$	mode	Refs
OG2	-1.317	17.41	0.15		
OG3	-1.206	16.65	0.63		
OG4	-1.305	16.72	0.32		
OG5	-1.184	16.79	0.36		
OG6	-1.295	17.20	0.19		
OG7	-1.333	17.17	0.12		
OG8	-1.379	16.75	0.25		
OG9	-1.306	16.95	0.40	F	
	-1.417			FO	
OG24	-1.274	17.19	0.20		
OG25	-1.359	17.14	0.07		
OG26	-1.413	17.35	0.08		
OG27	-1.277	17.05	0.10	F	
	-1.386			FO	
OG28	-1.442	16.74	0.05		
OG29	-1.410	17.31	0.05		
OG32	-1.313	16.99	0.25		
OG33	-1.422	17.43	0.08		
OG34	-1.420	17.38	0.05		
OG35	-1.400	17.35	0.08		
OG36	-1.425	17.40	0.08	FO	
	-1.521			SO	
OG37	-1.470	16.55	0.03		
OG38	-1.426	17.52	0.05		
OG39	-1.432	17.56	0.04		
OG40	-1.437	17.36	0.10		
OG42	-1.241	17.00	0.23		
OG45	-1.183	16.84	0.24		
OG46	-1.389	17.40	0.08		
OG50	-1.326	17.04	0.48		
OG59	-1.457	17.51	0.10	FO	
	-1.544			SO	
OG60	-1.391	17.47	0.06		
OG62	-1.331	17.46	0.06		
OG63	-1.398	17.32	0.08		
OG66	-1.426	17.53	0.07		
OG70	-1.335	17.08	0.05	FO	
	-1.426			SO	
<b>NGC 5272 M 3</b>					
Anon.	-1.509	18.36	0.08		NP96; NM90; Kal98
V237	-1.397	18.00	0.20		
NW858	-1.429	18.28	0.09		
SE174	-1.398	17.98	0.07		
NW449	-1.395	18.29	0.12		
<b>NGC 5466</b>					
NH 27	-1.295	18.72	0.14		NM90
NH 29	-1.395	18.86	0.16		

TABLE 4—*Continued*

Cluster Var.N.	logP	$\langle V \rangle$	$A_V$	mode	Refs
NH 35	-1.302	18.91	0.47		
NH 38	-1.258	18.80	0.46		
NH 39	-1.297	19.11	0.36		
NH 49	-1.347	19.20	0.25		
<b>IC 4499</b>					
S93-4	-1.253	19.3	0.30		RLG00
<b>NGC 5897</b>					
V9	-1.296	18.7	0.3		W96
<b>NGC 5904 M 5</b>					
V1	-1.375	17.48	0.11		KTKP99; RLG00
V2	-1.384	16.76	0.02		
V3	-1.380	17.04	0.08		
V4	-1.324	16.92	0.06		
V160	-1.047	15.3	0.1		
<b>NGC 6362</b>					
V38	-1.176	16.98	0.65		MKK99
V46	-1.3	17.48	0.05		
V47	-1.3	17.10	0.05		
V48	-1.3	17.01	0.05		
<b>NGC 6397</b>					
V10	-1.521	15.83	0.11		K97
V11	-1.418	15.34	0.04		
<b>NGC 6752</b>					
V7	-1.2286	15.59	0.46		TKPK99
V12	-1.3883	16.12	0.035		
V13	-1.3289	16.26	0.07		
<b>NGC 6809 M 55</b>					
V16	-1.272	16.94	0.02		RLG00
V17	-1.384	17.18	0.05		
V18	-1.332	16.98	0.03		
V19	-1.418	17.27	0.03		
V20	-1.479	17.04	0.10		
V21	-0.8677	15.76	0.04		
V22	-1.341	16.81	0.34		
V23	-1.383	17.22	0.05		
V24	-1.379	17.06	0.03		
V25	-1.007	15.88	0.90		
V26	-1.086	16.11	0.17		
V27	-1.387	17.09	0.03		
V31	-1.411	17.23	0.04		
V32	-1.382	16.92	0.10		
V33	-1.227	16.40	0.05		
V34	-1.432	17.23	0.03		
V35	-1.312	16.57	0.07		
V36	-1.405	16.74	0.07		
V37	-1.359	16.96	0.05		
V38	-1.418	16.69	0.04		

TABLE 4—*Continued*

Cluster Var.N.	logP	$\langle V \rangle$	$A_V$	mode	Refs
V39	-1.446	17.21	0.04		
V40	-1.432	17.20	0.03		
V41	-1.345	16.53	0.11		
V42	-1.435	17.16	0.05		
<b>NGC 6838 M 71</b>					
H1	-1.286	15.99	0.11		NM90
Dwarf Galaxies					
<b>Carina</b>					
V1	-1.197	22.70	0.30	FO	MHKN98; P99
V2	-1.340	23.10	0.45	?	
V3	-1.143	22.92	0.30	F	
V4	-1.246	23.02	0.45	F	
V5	-1.228	23.06	0.50	F	
V6	-1.155	22.79	0.35	F	
V7	-1.312	23.20	0.45	F	
V8	-1.253	23.23	0.50	F	
V9	-1.122	22.79	0.45	F	
V10	-1.229	23.03	0.45	F	
V11	-1.145	22.75	0.50	F	
V12	-1.256	22.83	0.35	FO	
V13	-1.173	22.93	0.60	F	
V14	-1.228	22.45	0.85	FO	
V16	-1.187	22.81	0.90	F	
V17	-1.187	22.95	0.70	F	
V18	-1.232	22.74	0.60	FO	
V19	-1.188	22.63	0.70	FO	
V20	-1.171	22.84	0.85	F	
<b>Sagittarius</b>					
V28	-1.269	20.61	0.26		RLG00
V29	-1.465	20.71	0.30		
V30	-1.249	20.35	0.26		
Galactic Field					
AE UMa	-1.065	11.27	0.6	F	H97a; R92
	-1.177			FO	
BE Lyn	-1.018	8.8	0.4	F	R90
RS Gru	-0.833	8.28	0.56	F	HP97
BS Tuc	-1.187	7.58	0.02	nr?	NM90
YZ Boo	-0.983	10.55	0.5	F	GCVS98
DY Peg	-1.137	10.38	0.54	F	NM90; W98
GP And	-1.104	10.75	0.55	F	L90
XX Cyg	-0.870	11.45	0.80	F	NM90
CY Aqr	-1.214	10.9	0.74	F	McN96; NM90
SX Phe	-1.260	7.33	0.77	F	HP97; NNL94
	-1.369			FO	
KZ Hya	-1.225	9.97	0.80	F	NM90; NNL94
BL Cam	-1.408	13.10	0.33	F	H97b
	-1.514			FO	

TABLE 4—*Continued*

Cluster	Var.N.	logP	$\langle V \rangle$	$A_V$	mode	Refs
---------	--------	------	---------------------	-------	------	------

<sup>a</sup>Nonradial variable, only the longest period is reported.

References: GCVS98 = "General Catalogue of Variable Stars" Kholopov et al. 1998; G98 = Gilliland et al. 1998; H97a = Hintz et al. 1997a; H97b = Hintz et al. 1997b; H&P97 = Hog & Petersen 1997; KK93 = Kaluzny & Krzeminski 1993; Kal96 = Kaluzny et al. 1996; Kal97 = Kaluzny et al. 1997; K97 = Kaluzny 1997; KKN97 = Kaluzny, Krzeminski & Nalezyty 1997; KKM95 = Kaluzny, Krzeminski & Mazur 1995; Kal98 = Kaluzny et al. 1998; KTKP99 = Kaluzny et al. 1999; L90 = Lopez De Coca et al. 1990; McN96 = McNamara et al. 1996; MHKN98 = Mateo, Hurley-Keller & Nemeč 1998; MKK99 = Mazur, Kaluzny & Krzeminski 1999a; NM90 = Nemeč & Mateo 1990; NNL94 = Nemeč, Nemeč & Lutz 1994; NP96 = Nemeč & Park 1996; P99 = Poretti 1999; PH98 = Petersen & Hög 1998b; R90 = Rodriguez et al. 1990; R92 = Rodriguez et al. 1992; TKPK99 = Thompson et al. 1999; W94 = Walker 1994; We96 = Wehlau et al. 1996; W98 = Wilson et al. 1998;

TABLE 5  
 LINEAR NONADIABATIC PERIODS AND PULSATION CONSTANTS ( $M/M_{\odot}=1.2$   $Z=0.001$ )

$L^a$ (1)	$T_e^b$ (2)	$\Pi_0^c/Q_0^d$ (3)	$\Pi_1/Q_1$ (4)	$\Pi_2/Q_2$ (5)	$\Pi_3/Q_3$ (6)	$\Pi_4/Q_4$ (7)	$\Pi_5/Q_5$ (8)	$\Pi_6/Q_6$ (9)
Y=0.24								
0.60	7900	3.2039(-2)	2.5203(-2)	2.0812(-2)	1.7474(-2)	1.4957(-2)	1.3014(-2)	...
...	...	3.1938(-2)	2.5123(-2)	2.0746(-2)	1.7419(-2)	1.4910(-2)	1.2973(-2)	...
0.77	8150	...	3.0173(-2)	2.4912(-2)	2.1061(-2)	1.8091(-2)	1.5786(-2)	1.3989(-2)
...	...	...	2.4627(-2)	2.0333(-2)	1.7190(-2)	1.4766(-2)	1.2884(-2)	1.1418(-2)
0.87	8150	...	3.5554(-2)	2.9137(-2)	2.4599(-2)	2.1144(-2)	1.8491(-2)	1.6428(-2)
...	...	...	2.4417(-2)	2.0010(-2)	1.6894(-2)	1.4521(-2)	1.2699(-2)	1.1282(-2)
0.98	7900	6.0973(-2)	4.7300(-2)	3.8532(-2)	3.2394(-2)	2.7845(-2)	2.4414(-2)	2.1736(-2)
...	...	3.1534(-2)	2.4462(-2)	1.9928(-2)	1.6753(-2)	1.4401(-2)	1.2626(-2)	1.1241(-2)
1.02	7600	7.3864(-2)	5.7443(-2)	4.6666(-2)	3.9114(-2)	3.3640(-2)	2.9549(-2)	...
...	...	3.1567(-2)	2.4549(-2)	1.9943(-2)	1.6716(-2)	1.4377(-2)	1.2628(-2)	...
1.05	7300	8.7692(-2)	6.8330(-2)	5.5417(-2)	4.6376(-2)	3.9946(-2)	...	...
...	...	3.1630(-2)	2.4646(-2)	1.9988(-2)	1.6727(-2)	1.4408(-2)	...	...
1.07	7000	1.0275(-1)	8.0149(-2)	6.4918(-2)	5.4314(-2)	...	...	...
...	...	3.1714(-2)	2.4737(-2)	2.0036(-2)	1.6763(-2)	...	...	...
1.08	6850	1.1160(-1)	8.7056(-2)	7.0466(-2)	...	...	...	...
...	...	3.1768(-2)	2.4781(-2)	2.0059(-2)	...	...	...	...
1.08	6700	1.2078(-1)	9.4215(-2)	7.6230(-2)	...	...	...	...
...	...	3.1829(-2)	2.4828(-2)	2.0088(-2)	...	...	...	...
1.09	6400	1.4208(-1)	1.1077(-1)	...	...	...	...	...
...	...	3.1990(-2)	2.4941(-2)	...	...	...	...	...
Y=0.30								
1.14	8000	...	...	...	...	3.0706(-2)	2.6860(-2)	2.3840(-2)
...	...	...	...	...	...	1.4448(-2)	1.2638(-2)	1.1217(-2)
1.14	7900	...	...	...	3.7149(-2)	3.1889(-2)	2.7895(-2)	2.4757(-2)
...	...	...	...	...	1.6802(-2)	1.4423(-2)	1.2616(-2)	1.1197(-2)
1.14	7800	...	...	4.6046(-2)	3.8663(-2)	3.3211(-2)	2.9077(-2)	2.5821(-2)
...	...	...	...	2.0033(-2)	1.6820(-2)	1.4448(-2)	1.2650(-2)	1.1233(-2)
1.15	7600	...	6.1544(-2)	5.0032(-2)	4.1952(-2)	3.6029(-2)	3.1547(-2)	2.8000(-2)
...	...	...	2.4669(-2)	2.0054(-2)	1.6816(-2)	1.4442(-2)	1.2645(-2)	1.1223(-2)
1.18	7300	...	8.6079(-2)	6.9654(-2)	5.8082(-2)	4.9782(-2)	4.3491(-2)	...
...	...	...	2.4862(-2)	2.0118(-2)	1.6775(-2)	1.4379(-2)	1.2561(-2)	...
1.18	7000	1.2621(-2)	9.8304(-2)	7.9434(-2)	6.6170(-2)	5.6688(-2)	...	...
...	...	3.2022(-2)	2.4942(-2)	2.0154(-2)	1.6789(-2)	1.4382(-2)	...	...
1.19	6700	1.4588(-1)	1.1360(-1)	9.1716(-2)	7.6447(-2)	...	...	...
...	...	3.2149(-2)	2.5035(-2)	2.0213(-2)	1.6848(-2)	...	...	...
1.19	6400	1.6881(-1)	1.3134(-1)	1.0603(-1)	...	...	...	...
...	...	3.2276(-2)	2.5112(-2)	2.0273(-2)	...	...	...	...

<sup>a</sup> Logarithmic luminosity (solar units). <sup>b</sup> Effective temperature (K). <sup>c</sup> Fundamental and overtone periods (d). <sup>d</sup> Fundamental and overtone pulsation constants (d).



